Warm climate isotopic simulations: What do we learn about interglacial signals in Greenland ice cores?

L.C. Sime, Camille Risi, J.C. Tindall, J. Sjolte, E.W. Wolff, Valérie Masson-Delmotte, E. Capron

Warm climate isotopic simulations: What do we learn about interglacial signals in Greenland ice cores?

Louise C. Sime[a], Camille Risi[bf], Julia C. Tindall[c], Jesper Sjolte[dg], Eric W. Wolff[a], Valérie Masson-Delmotte[e], Emilie Capron[a]

[a] *British Antarctic Survey, Cambridge, CB3 0ET, U.K.*
[b] *Cooperative Institute for Research in Environmental Sciences, University of Colorado, Boulder, U.S.A.*
[c] *School of Earth and Environment, University of Leeds, Leeds, LS2 9JT, U.K.*
[d] *Niels Bohr Institute, Centre for Ice and Climate, University of Copenhagen, Juliane Maries Vej 30, DK-2100 Copenhagen, Denmark*
[e] *Laboratoire des Sciences du Climat et de l'Environnement (UMR 8212 CEA-CNRS-UVSQ), Gif-sur-Yvette, France*
[f] *Laboratoire de Météorologie Dynamique (IPSL/CNRS/UPMC), Paris, France*
[g] *GeoBiosphere Science Centre, Quaternary Sciences, Lund University, Slvegatan 12, SE-223 62 Lund, Sweden*

Abstract

Measurements of last interglacial stable water isotopes in ice cores show that central Greenland $\delta^{18}O$ increased by at least 3 ‰ compared to present day. Attempting to quantify the Greenland interglacial temperature change from these ice core measurements rests on our ability to interpret the stable water isotope content of Greenland snow. Current orbitally driven interglacial simulations do not show $\delta^{18}O$ or temperature rises of the correct magnitude, leading to difficulty in using only these experiments to inform our understanding of higher interglacial $\delta^{18}O$. Here, analysis of greenhouse gas warmed simulations from two isotope-enabled general circulation models, in conjunction with a set of last interglacial sea surface observations, indicates a possible explanation for the interglacial $\delta^{18}O$ rise. A reduction in the winter time sea ice concentration around the northern half of Greenland, together with an increase in sea surface temperatures over the same region, is found to be sufficient to drive a > 3 ‰ interglacial enrichment in central Greenland snow. Warm climate $\delta^{18}O$ and δD in precipitation falling on Greenland are shown to be strongly influenced by local sea surface condition changes: local sea surface warming and a shrunken sea ice extent increase the proportion of water vapour from local (isotopically enriched) sources, compared

to that from distal (isotopically depleted) sources. Precipitation intermittency changes, under warmer conditions, leads to geographical variability in the $\delta^{18}O$ against temperature gradients across Greenland. Little sea surface warming around the northern areas of Greenland leads to low $\delta^{18}O$ against temperature gradients (0.1-0.3 ‰ per °C), whilst large sea surface warmings in these regions leads to higher gradients (0.3-0.7 ‰ per °C). These gradients imply a wide possible range of present day to interglacial temperature increases (4 to >10°C). Thus, we find that uncertainty about local interglacial sea surface conditions, rather than precipitation intermittency changes, may lead to the largest uncertainties in interpreting temperature from Greenland ice cores. We find that interglacial sea surface change observational records are currently insufficient to enable discrimination between these different $\delta^{18}O$ against temperature gradients. In conclusion, further information on interglacial sea surface temperatures and sea ice changes around northern Greenland should indicate whether +5°C during the last interglacial is sufficient to drive the observed ice core $\delta^{18}O$ increase, or whether a larger temperature increases or ice sheet changes are also required to explain the ice core observations.

Keywords: Greenland, interglacials, atmospheric modelling, stable water isotopes, ice cores

1. Introduction

Stable water isotope measurements, $\delta^{18}O$ and δD, in polar ice cores provide valuable information on past temperature. A main control on the distribution of $\delta^{18}O$ (and equivalently, for this case, δD) in preserved ice in Greenland is local temperature (Dansgaard, 1964). Thus the stable water isotopic content of ice cores can be used as an indicator of past temperature.

Understanding last interglacial temperature across Greenland could help with assessing the impacts of a shrunken Greenland ice sheet (*e.g.* Letreguilly et al., 1991; Chen et al., 2006; Velicogna, 2009; Vinther et al., 2009; Colville et al., 2011), and may offer an opportunity to understand how aspects of the Earth system (*e.g.* sea ice and ocean temperatures) behave in a period of Arctic warmth (*e.g.* Cuffey and Marshall, 2000; Johnsen et al., 2001; NGRIP Project Members, 2004; Masson-Delmotte et al., 2006; Vinther et al., 2009; Turney and Jones, 2010; Masson-Delmotte et al., 2010).

The current longest well dated undisturbed Greenland ice core record

of $\delta^{18}O$ published is 123 ka long and is from NorthGRIP (NGRIP Project Members, 2004). However the peak of the last interglacial is thought to have occurred between 125 and 130 thousand years before present (ky), most likely at about 126 ky (Otto-Bliesner et al., 2006; Masson-Delmotte et al., 2011). The NorthGRIP record therefore contains no isotopic information from the early part of the last interglacial. The high $\delta^{18}O$ value at 123 ka nevertheless suggests that the temperature in the last interglacial part of the record was substantially warmer than at any time in the Holocene.

In order to make the link between climate change and $\delta^{18}O$ responses, it is necessary to understand climatic impacts on $\delta^{18}O$ across Greenland. Greenland $\delta^{18}O$ measurements have been traditionally converted into temperature using the linear relationship (*e.g.* $\delta^{18}O = aT + b$, where T is the surface temperature) derived from spatial information (Dansgaard, 1964; Jouzel et al., 1994, 1997). Spatial observations of $\delta^{18}O$ and temperature show a strong linear relationship with a gradient, for inland sites, of about 0.7 to 0.8 ‰ per °C (Johnsen et al., 1995; Sjolte et al., 2011). However, since evaporation conditions, transport pathways, and site elevation changes also effect $\delta^{18}O$, there are many reasons why temporal gradients, and hence the interpretation of temperature shifts through time, may differ from the spatial gradients (see also *e.g.* Dansgaard, 1964; Jouzel et al., 1997; Noone and Simmonds, 2004; Helsen et al., 2007; Schmidt et al., 2007; Sime et al., 2008; Noone, 2008; Cuffey and Paterson, 2010).

Alternative information that can be used to help understand how the $\delta^{18}O$ record has varied with past Greenland temperature is available from the temperature profile measured in the borehole (Cuffey et al., 1995; Johnsen et al., 1995; Dahl-Jensen et al., 1998), and from measurements of the isotopic composition of the air trapped in ice (Severinghaus et al., 1998; Severinghaus and Brook, 1999; Capron et al., 2010; Kobashi et al., 2011). The temporal gradients obtained in these studies are generally significantly smaller than the spatial gradients. Values range from 0.23 to 0.55 ‰ per °C, with most values falling around 0.3 ‰ per °C. Interestingly, despite this evidence, papers discussing the last interglacial record have nevertheless generally used the 0.7 ‰ per °C gradient (which implies that +3.5 ‰ in $\delta^{18}O$ might be interpreted as equivalent to +5°C shift in temperature) to infer past temperature shifts (*e.g.* NGRIP Project Members, 2004).

For a past warmer interglacial climate, where the temperature information from the borehole and isotopic measurements from trapped air are not available, a possible alternative test of temporal gradients is to calculate $\delta^{18}O$

and temperature values over a range of climates using an isotopically enabled general circulation model (GCM) (*e.g.* Jouzel et al., 1994; Sime et al., 2008). For cold climate shifts, the isotopic signal in ice cores in Greenland seem to be more biased towards summer snow (Krinner and Werner, 2003); though it is worth noting that the sign and magnitude of this biasing or precipitation intermittency change effect does vary between models. Similar biasing issues also appear to occur in Antarctica under warmer climates (Sime et al., 2009b). Model based results have thus been used as an explanation of low (0.3-0.4 ‰ per °C) $\delta^{18}O$ against temperature gradients for past climate cold-shifts across Greenland (Krinner et al., 1997; Werner et al., 2000).

For Greenland, the temperature and isotopic increases simulated across Greenland using an ocean-atmosphere GCM forced only by interglacial orbital and greenhouse gas forcing are very small; the Masson-Delmotte et al. (2011) isotopic shift amounts to less than 20% of the observed interglacial isotopic shift. The implies that these simulations are not yet in good agreement with observational constraints, and that it is difficult to use only these orbitally-driven simulations to help understand interglacial $\delta^{18}O$ in ice cores. Here we therefore complement the Masson-Delmotte et al. (2011) orbital approach with the detailed investigation of isotopic climate simulations warmed by greenhouse gas forcing. In using this method we are not trying to use the greenhouse gas (GHG) driven simulations as a direct analogue for last interglacial, rather the approach allows investigation of the isotopic response to patterns of sea surface warming and sea ice change.

In overview, the manuscript first compiles last interglacial Greenland isotopic and Atlantic and Arctic sea surface observations. Secondly, we present a brief discussion of the isotopic models and GHG driven simulations. Third, simulation results are presented in two parts. Present day simulation results are compared to present day Greenland observations, then the warmer simulation results are presented and discussed. Fourth, we consider what we can learn from the warmer simulation results, in the context of last interglacial sea surface observations, about the interpretation of last interglacial ice in Greenland cores. Finally, the last section summarises our findings and draws together some conclusions.

2. Interglacial observations from Greenland and its surrounding region

In comparison with present day, Holocene, or even last glacial conditions, the amount of information about the last interglacial peak (around 125-130 ky) is rather limited (*e.g.* Johnsen et al., 2001; MARGO Project Members, 2009; Leduc et al., 2010). An overview of the currently available last interglacial observations for Greenland ice cores, and for near Greenland sea surface condition observations, is provided below. Note, observations of present day temperature, accumulation, and $\delta^{18}O$ from ice core tops and other surface sites across Greenland are provided in Appendix B.

2.1. Interglacial Greenland ice core observations:

There is currently no complete record of the last interglacial from Greenland ice cores. However, there are four publicly available Greenland stable water isotope ice core records that may feature some last interglacial ice (Fig. 1b). The $\delta^{18}O$ isotopic records from NGRIP, GRIP, Renland, DYE3, and Camp Century show similar variations over the majority of the last glacial period. This strongly suggests that the upper parts of these cores depict continuous undisturbed climatic records. However, the lack of agreement between their bottom parts implies that stratigraphic disturbances perturb their respective depth-age relationships. See Fig. 1 for positions and $\delta^{18}O$ records. Fig. 1a also shows the maximum difference in $\delta^{18}O$ between present day (0-3 ky average) and the 'last interglacial' maximum (the highest value in Fig. 1b which occurs before 100 ky).

Of the available Greenland ice core records, NGRIP is the only site which provides a continuous undisturbed climatic record back to the last interglacial. However, bedrock was reached at 3085 m and the deepest ice is thought to be 123 ky old (NGRIP Project Members, 2004; Landais et al., 2005). Thus, the NGRIP ice core probably does not record the maximum peak of the last interglacial. At GRIP the lowest 10% of the core, older than 110 ky, has a disturbed stratigraphy (Landais et al., 2003; Suwa et al., 2006). While the observed $\delta^{18}O$ at the bottom of the core suggests the presence of interglacial ice (Fig. 1), there is doubt whether peak interglacial $\delta^{18}O$ values are represented (GRIP Project Members, 1993; Johnsen et al., 2001; Suwa et al., 2006). The Renland record has a depth-age model only until 60 ky (Svensson et al., 2008). For simplicity, the isotopically lightest near bed Renland ice is placed at 123 ky, however it is likely that this also does

not represent a peak interglacial value. For DYE3, there is also no available depth-age model for the deep ice, and evidence of silt in this core bottom ice means that the maximum old ice $\delta^{18}O$ could be representative of something other than precipitation directly over the site (Langway et al., 1985; Johnsen et al., 2001). A fifth Greenland ice core $\delta^{18}O$ record was obtained from Camp Century in north west Greenland around 1972 (Johnsen et al., 1972). Although we do not have the measurements available to place Camp Century values on Fig. 1b, this site also appears to contain some last interglacial ice (Johnsen et al., 2001). The magnitude of the present day to last interglacial Camp Century peak changes in $\delta^{18}O$ seems similar to those from the more central (NGRIP, GRIP, and Renland) sites, at between + 3 and + 5 ‰ (Johnsen et al., 2001; NGRIP Project Members, 2004).

A conservative summary of the available $\delta^{18}O$ records is simply that between the present day and the peak of the last warm interglacial (somewhere between 125-130 ky), there was an increase in $\delta^{18}O$ of at least 3 ‰ in central and north-western Greenland. For southern and eastern Greenland $\delta^{18}O$ variations suggest that last interglacial values were also higher (Fig. 1b), but the values seem currently too uncertain to be used as individual quantitative observational constraints.

2.2. Interglacial sea surface condition observations:

Available observations used to reconstruct maximum last interglacial sea surface temperatures from various paleoclimatic archives were compiled by Turney and Jones (2010). A compilation considering the maximum temperature peak may not be reflective of any one single last interglacial climatic period (Lang and Wolff, 2010; Govin et al., 2012). Thus there is doubt over whether these peak reconstructed sea surface interglacial temperatures are co-incident everywhere across the Northern Hemisphere. Table 2 presents the rather sparse set of available qualitative observations of last interglacial sea ice changes from across the Northern Hemisphere. Please see Section 5 for analysis and discussion of these last interglacial sea surface temperature and sea ice observational constraints.

3. Isotopic Modelling

Two sets of atmospheric general circulation model (AGCM) simulations are used in this study of climate and isotopes in precipitation over Greenland (Table 1). We wish to simulate the observed magnitude of the last in-

terglacial Greenland $\delta^{18}O$ shift. Since an orbitally driven approach appears to fail to drive the correct magnitude of $\delta^{18}O$ increase (Masson-Delmotte et al., 2011), we use GHG-forced simulations from different coupled models, which feature contrasting sea surface temperature responses. We are not trying to use these GHG driven simulations as a direct analogue for last interglacial, nevertheless the approach allows insight into the interpretation of interglacial isotopic changes across Greenland. One set of experiments uses the isotopically enabled HadAM3 atmospheric model, and one uses the isotopically enabled atmospheric LMDZ4 model. Using two models allows us to also investigate whether differing atmospheric physics between the models affects our findings.

3.1. The use of greenhouse gas forced simulations:

Our goal here is to investigate the isotopic response to different patterns of warming, which may be of a magnitude similar to those of the last interglacial. It is useful if these patterns are diverse; diversity increases the likelihood that we encompass the last interglacial pattern.

Our warm climate simulations are driven by greenhouse gas (GHG), rather than interglacial orbital forcing. Note, as in Sime et al. (2008) CO_2 and GHG driven warming are used interchangeably *i.e.* where CO_2 is written, we wish to imply CO_2 equivalent GHG forcing. The use of the GHG warming, rather than orbital forcing, as noted in the introduction, is done for three main reasons. Firstly, the amount of annual mean warming across Greenland in the Masson-Delmotte et al. (2011) orbitally forced simulation is very small (+0.9°C at 126 ky). Although the interglacial orbitally-driven summer warming, of close to 5°C, agrees with some available summer observations (CAPE Project Members, 2006), the annual mean warming of 0.9°C is very small (less than 20%) compared with previous temperature reconstructions (NGRIP Project Members, 2004).

Secondly, the Greenland isotopic shift in the orbitally forced simulations is very small, at around + 0.1 to + 0.5 ‰ of $\delta^{18}O$ (Masson-Delmotte et al., 2011). This simulated shift amounts to less than 20% of the observed interglacial isotopic shift (Fig. 1). The small orbitally forced interglacial Greenland temperature and isotopic shifts lead to difficulty in interpreting temporal $\delta^{18}O$ against temperature gradients. This is because the geographical variability in temporal gradients (see also Sime et al., 2009b) between these orbital-interglacial and present day experiments is large (two orders of magnitude larger than in the GHG forcing, see section 4.5) in these experiments

(not shown). Effectively, the low climate signal to climate noise ratio means that interpretation of the climate-isotope signal is extremely difficult.

A third reason it is useful to focus on the GHG forced experiments is the large differences between the coupled model sea surface boundary changes (see Section 4.2 for details and results). Many differences in coupled model results can be attributed to the difficulty associated with modelling oceans during non-present day climate periods: for example, present parameterisations of ocean mixing may mean that current ocean models are not well suited to simulating climate periods when the ocean is in a different state (Wunsch, 2003; Watson and Naveira Garabato, 2006). Additionally, sea ice is quite poorly represented leading to large biases in high latitude results (*e.g.* Stroeve et al., 2007). These known modelling problems may contribute to the cold and low $\delta^{18}O$ biases in the Masson-Delmotte et al. (2011) simulated interglacial climate. However, here these deficiencies are turned to advantage. The HadCM3 and IPSL sea surface differences (mainly due to ocean and sea ice model differences) enable examination of the impact of different warm climate sea surface boundary changes on atmospheric simulations.

3.2. The use of two isotopic AGCMs:

The isotopically enabled AGCMs HadAM3 (isotopic version 1.0, unified model version 4.5) and LMDZ4 both have a regular latitude longitude grid, with a resolution of 2.5 ° × 3.75 °, and 19 hybrid coordinate levels in the vertical (Pope et al., 2000; Risi et al., 2010). Tindall et al. (2009) and Risi et al. (2010) present details of the stable water isotopic submodels that were incorporated into HadAM3 and LMDZ4, respectively. The use of two separate atmospheric isotopic models is helpful for checking whether our results are model specific.

3.3. The isotopic simulations:

The HadAM3 and LMDZ4 control isotopic simulations are based on similar sets of present day sea surface observations (Table 1). The present day period is used as a control because we can test these simulation results against a set of present day Greenland snow $\delta^{18}O$ observations.

For the warmer than present day simulations, coupled ocean-atmosphere versions (HadCM3 and IPSL version CM4) of the respective AGCM are used to simulate warmer than present day climates. The main warmer simulations are driven by similar GHG forcings. Additional very warm simulations driven

by larger GHG forcings are also used. Two additional experiments also simulate the individual effects of the warmer sea surface temperatures (SST) and sea ice changes (SeaIce).

The sea surface temperature anomalies from each coupled model simulation are applied to the control sea surface temperatures. The atmospheric only, but isotopically enabled, version of the AGCM is then run. This use of sea surface temperature anomalies reduces the impact of known model errors (Krinner et al., 2008; Sime et al., 2008; Masson-Delmotte et al., 2011). All the simulations use fixed (present day) Greenland ice sheet elevations. See Appendix A for more detail on the simulations.

4. Isotopic simulation results

Firstly, a check of the HadAM3 and LMDZ4 present day simulation results is presented. This is useful to help assess the validity of model-data comparisons. To help understand what aspects of the warmer climate changes drive the isotopic changes, analysis of isotopic and climatic changes between the present day and warmer simulations is then presented. The following discussion section brings the model analysis together with observational constraints, and provides an overview of climate insights gleaned from the analysis.

4.1. The present day simulation of Greenland ice sheet climate

Here a brief overview of the model climatology and isotopic results over Greenland is given. See Appendix B for a more detailed comparison between available observations and present day simulation values (using co-located model results).

Table 3 provides present day simulation results using the Masson-Delmotte et al. (2006, 2011) definition of central Greenland *i.e.* using all points higher than 1300 m. Using this >1300 m definition, present day central Greenland HadAM3 temperatures are -24.0°C whilst LMDZ4 values are -18.8°C (Fig. 2a and 3a). Annual mean precipitation across the whole central Greenland region for the HadAM3 simulation is 325.8 kg m^{-2} yr^{-1}, the LMDZ4 results are wetter at 454.0 kg m^{-2} yr^{-1} (Fig. 2b and 3b). Both HadAM3 and LMDZ4 show that the overall geographical pattern of observations and simulation results compare quite well (Fig. 2ab and 3ab). HadAM3 temperature and precipitation value are likely more reflective of the observed Greenland climate than LMDZ4 (Appendix B), but in common with other

models (Sjolte et al., 2011), the simulated precipitation in both models in southern Greenland is too high (*e.g.* Burgess et al., 2010). Like some other isotopic model simulations of Greenland (*e.g.* Hoffmann and Heimann, 1998; Sjolte et al., 2011), the annual mean isotopic values of the precipitation, in HadAM3 and LMDZ4, are heavier than the observations (Fig. 2c and 3c). This could be related to a warm bias (Sjolte et al., 2011), and possibly also some difficulties in the accurate simulation of seasonal cycles (Appendix B). In general, despite a reasonable orographic representation of central Greenland (Fig. 2f and 3f) and reasonable simulated precipitation, differences in model-observation seasonality and $\delta^{18}O$ do suggest that the origin and pathways of water to Greenland are, as for other models, also probably not fully accurate for either HadAM3 or LMDZ4.

4.2. Warmer climate simulation results for Greenland.

Here, changes between the present day and main warmer simulations are presented. The HadAM3 SRES A1B and A2 simulations are differenced to the HadAM3 present day simulations. The LMDZ4 CO2 $\times$ 2 and 4 simulations are differenced against the LMDZ4 present day simulation. See Table 3 for a summary of simulated mean annual central Greenland changes.

4.2.1. Mean annual changes:

Fig. 4 shows $\delta^{18}O$ changes between the HadAM3 and LMDZ4 warmer and present day simulations (left hand panels). The central Greenland $\delta^{18}O$ changes for HadAM3 A1B simulations (Fig. 4ab) and for the warmest LMDZ4 CO2 $\times$ 4 simulation (Fig. 4gh) both show changes of +3.6 and +1.8 ‰ in $\delta^{18}O$, respectively. These values are comparable to the observed interglacial $\delta^{18}O$ increase in central Greenland (Fig. 1).

For the HadAM3 SRES A1B simulation, mean annual results (central Greenland >1300 m), mean central Greenland temperature and precipitation changes between the present day and warmer simulation are: +4.7°C and +93 kg m^{-2} yr^{-1}, and an enrichment in $\delta^{18}O$ of +3.6 ‰. For the warmer HadAM3 SRES A2 simulation, mean central Greenland temperature and precipitation changes by: +5.4°C and +117.1 kg m^{-2} yr^{-1}, and an enrichment in $\delta^{18}O$ of +3.9 ‰ occurs. Both of the warmer HadAM3 simulations shown in Fig. 4 display quite large changes in the isotopic values. The spatial pattern of changes in $\delta^{18}O$ is closely related to changes in temperature and precipitation for these simulations (Fig. 4).

For the LMDZ4 CO2 $\times$ 2 simulation, mean central Greenland temperature and precipitation changes are: +3.3°C and +74.1 kg m^{-2} yr^{-1}, but the enrichment in $\delta^{18}O$ is quite small at 0.31 ‰. For the warmer LMDZ4 CO2 $\times$ 4 simulation mean central Greenland temperature and precipitation changes are: +7.3°C and +176.1 kg m^{-2} yr^{-1} in precipitation, with a larger enrichment in $\delta^{18}O$ of +1.8 ‰. So, although the temperature and precipitation changes for these LMDZ4 simulations are comparable to the HadAM3 changes, the LMDZ4 simulations feature smaller isotopic changes. The d-excess changes for LMDZ4, like the $\delta^{18}O$ changes, are also smaller than those associated with the HadAM3 simulations (Fig. 4).

It is difficult to interpret the d-excess results. HadAM3 and LMDZ each use a slightly different representation of micro-scale cloud physics (Tindall et al., 2009; Risi et al., 2010). This difference in supersaturation tuning has little impact on either first order $\delta^{18}O$ or δD, but it does affect second order d-excess (Schmidt et al., 2007; Werner et al., 2011). Better model representations of these aspects of micro-scale cloud physics would be helpful in allowing a more insightful analysis of d-excess observations (Noone and Sturm, 2010).

The pattern of temperature, precipitation, and $\delta^{18}O$ changes suggest a relationship between the climate driven isotopic response over Greenland and the sea surface conditions in the vicinity of Greenland (Fig. 4). The HadAM3 simulations tend to show a larger degree of warming, precipitation change, and isotopic change in the central northern regions of Greenland, particularly towards the east. This ties in with larger sea surface temperature and sea ice changes towards the north and east. Changes in d-excess (Fig. 4, right panels, shaded over Greenland) also show similarity to temperature and $\delta^{18}O$ changes (Fig. 4, left panels, contoured and shaded) and a weaker similarity to precipitation changes.

For every model simulation, southern regions of Greenland show smaller changes in temperature, precipitation, $\delta^{18}O$, and d-excess (Fig. 4). This is likely related to the relatively small changes in sea surface conditions surrounding this region of Greenland.

4.2.2. Seasonal changes:

There is a strong seasonal relationship between changes in temperature and $\delta^{18}O$ (Fig. 5). The monthly changes in precipitation are also visually closely tied to the temperature changes, but monthly d-excess shows a different pattern. Fig. 6 shows a selection of possible predictors of isotopic

changes. The subsequent section examines causation, however here we simply regress the anomalous monthly $\delta^{18}O$ and d-excess (Fig. 5) on pairs of these possible predictors (Fig. 6) to examine correlations on the seasonal timescale. HadAM3 monthly $\delta^{18}O$ changes are strongly correlated with local SST and evaporation changes (up to 86% of monthly $\delta^{18}O$ variance is explained). LMDZ4 monthly $\delta^{18}O$ changes are better correlated with broader North Atlantic region changes in evaporation and sea surface conditions (up to 62% of monthly $\delta^{18}O$ variance explained). The monthly d-excess anomalies for LMDZ4 are strongly correlated with local evaporation and higher sea surface temperature (up to 85% of variance explained), whilst HadAM3 d-excess is more closely related to wider North Atlantic evaporation and sea ice changes (up to 67% of variance explained). In summary, whilst HadAM3 and LMDZ4 isotopes seem to respond slightly differently to different seasonal climate changes, in both models $\delta^{18}O$ and d-excess tend to respond most strongly to: local temperature; sea surface temperature; sea ice changes; and evaporation.

4.3. The impact of surface conditions and source effects

Section 4.2 suggests that sea surface condition changes are key to understanding changes in $\delta^{18}O$ in Greenland snow. Here, additional HadAM3 sensitivity simulations and LMDZ4 source tracking simulations are presented to help clarify mechanisms. Two sensitivity simulations were performed where the sea surface temperatures and sea ice changes were applied individually (Table 1). The differences between Fig. 7a and Fig. 7c suggest that the applied sea surface temperature changes tend to raise the inland temperatures and $\delta^{18}O$ values more than the sea ice changes do, but Fig. 7b and Fig. 7d (contours) suggests that in the north-east Greenland the precipitation changes are approximately equally dependent on both the sea surface temperature and sea ice changes.

Comparison of the HadAM3 SeaIce (warm climate sea ice retreat but no sea surface temperature change, Fig. 7cd) and LMDZ4 CO2 $\times$ 2 and $\times$ 4 results (Fig. 4efgh) shows several similarities. The sea surface condition changes around Greenland in LMDZ4 CO2 $\times$ 2 and CO2 $\times$ 4 are closer to HadAM3 SeaIce simulation than the A1B simulation; the sea surface temperatures change not much (or not at all) in each of these LMDZ4 experiments around the northern edge of Greenland. A substantial loss of sea ice around Greenland however does occur in each of these simulations. As a result, the isotopic responses in central Greenland for both LMDZ4 simulations are

similar to the HadAM3 SeaIce sensitivity simulation. Appendix C confirms that these sea surface conditions are the main drivers of the model isotopic response; differences in model physics are relatively unimportant. In each case, the $\delta^{18}O$ enrichment (Fig. 4e), the d-excess change patterns (Fig. 4fh), and the $\delta^{18}O$ - against temperature gradients (see Table 3) are similar. This is particularly apparent when comparing the HadAM3 SeaIce and LMDZ4 CO2 $\times$ 4 model simulations.

The difference between Fig. 4ab and Fig. 7ef indicates that the Fig. 4ab pattern and magnitude of changes in temperature, precipitation, $\delta^{18}O$, and d-excess can neither be fully replicated by simulations which apply the sea surface temperature changes (Fig. 7ab) nor just the sea ice changes (Fig. 7cd): applying the changes in sea surface temperature or sea ice separately is not equivalent to applying both changes simultaneously. The isotopic response (shading over Greenland) for the SST + SeaIce is smaller than for SST and SeaIce changes combined (*i.e.* the A1B Fig. 4ab results). This indicates that there are some non-linearities in the response of Greenland temperature, precipitation, $\delta^{18}O$, and d-excess to reductions in sea ice and sea surface temperature increases.

4.4. Precipitation source effects on isotopic values:

Whilst Section 4.2 and 4.3 both emphasise that sea surface temperature and sea ice changes strongly affect isotopic changes over Greenland, Section 4.3 also indicates that joint (non-linear) effects of sea surface temperature and sea ice changes together drive larger isotopic changes. One of the possible ways in which non-linear behaviour may impact on $\delta^{18}O$ is through sea surface evaporation effects (Masson-Delmotte et al., 2005). For high latitudes, Noone (2008) shows that if the proportion of precipitation vapour sourced from local sea surface local regions increases, isotopic enrichment of precipitation tends to occur. Source changes therefore can change the isotopic composition of Greenland snow (*e.g.* Hoffmann and Heimann, 1997; Noone, 2008; Masson-Delmotte et al., 2011).

Source tracking is useful in allowing the origin of precipitation over Greenland to be ascertained (see Appendix C for technical details). The experiments outlined in 3.3.2 are therefore also run with the LMDZ4 model using the source-tracking feature (see Appendix D for details). Precipitation sources over Greenland are divided into three regions: high latitude (sea surface north of 50°N); mid-low latitude (sea surface south of 50°N); and

continental (from all continental regions). Using the same central Greenland definition as in Section 4.1 above, the source tracking results indicate that most present day central Greenland precipitation is sourced from mid-low latitude regions (51 %), with lesser amounts originating from more local high-latitude (19%) and continental (30%) regions (Table 4). Table 4 indicates that mid-low latitude and continental region sourced precipitation tends have a depleted $\delta^{18}O$ value, of around -30 to -40 ‰, whilst the (local) high-latitude sourced precipitation is substantially more enriched, at around $+2$ to $+5$ ‰.

Analysis of results for these additional source tracked simulations shows quite different changes in precipitation sources. The strong sea surface temperature warming north of Greenland in HadCM3 generates a substantial (approx 15%) increase in the percentage of high-latitude precipitation across northern Greenland (Fig. 8a). In contrast to this, the strong mid-low latitude sea surface temperature warming and much smaller changes around Greenland produced by IPSL, leads to a large percentage reduction (approx $-$ 15%) in high-latitude precipitation across the whole of Greenland. Precipitation in this simulation instead becomes more influenced by mid-low latitude and continentally sourced precipitation. This difference between the two model simulations is important because it means more distal $\delta^{18}O$ depleted vapour is present in the warmer LMDZ4-IPSL simulations. This will tend to deplete $\delta^{18}O$ value in snow. Whereas for HadAM3-HadCM3, the larger proportion of more local high-latitude vapour across northern Greenland tends to enrich the simulated warmer climate $\delta^{18}O$ values.

4.5. Isotope against temperature gradients

Despite reasonable similarity in the amount of warming across the AGCM simulations, there is a wide range of temporal $\delta^{18}O$ against temperature gradients (Table 3). The HadAM3 simulations yield mean central Greenland gradients of 0.76 and 0.71 ‰ per °C for the A1B and A2 simulations, respectively. For LMDZ4, the CO2 $\times$ 4 simulation gradient is much lower at 0.25 ‰ per °C.

In addition to the mean gradient differences between the simulations, it is also of interest to look at what causes geographical variability in the temperature against $\delta^{18}O$ relationship across Greenland. Since $\delta^{18}O$ is recorded in precipitation, and is therefore 'precipitation-weighted', we also briefly compare $\delta^{18}O$ change with precipitation-weighted surface temperature change for each location. Various authors (*e.g.* Krinner et al., 1997; Werner and

Heimann, 2002; Krinner and Werner, 2003; Sime et al., 2008, 2009a) have shown that precipitation weighted temperature changes can deviate significantly from temperature changes. Geographical differences between temperature and precipitation weighed temperature anomalies can be important for understanding geographical variations in temporal $\delta^{18}O$ against temperature gradients (Sime et al., 2009b). The weighting is done here using daily precipitation and temperature values. See Sime et al. (2008) for details of the calculation. (The difference between temperature and precipitation weighted temperature is sometimes called 'precipitation biasing'.) Additional checks using a subset LMDZ4 results, provided in Appendix C, confirm these HadAM3 results also apply to LMDZ4.

Fig. 9 shows the $\delta^{18}O$ against temperature gradients for each model simulation (shaded). For the HadAM3 simulations, the contours show the associated changes in precipitation biasing. Each model simulation shows geographical variability in the $\delta^{18}O$ against temperature gradient. The available HadAM3 and LMDZ4 (Appendix C) precipitation biasing results suggest that much of this geographical variability is due to geographical-climate variability in precipitation intermittency (Fig. 9abef). Additional continental-scale geographical variability is also driven by local sea surface condition control of $\delta^{18}O$ (see Fig. 4, and previous sections).

In summary, whilst there is some Greenland geographical variability within the simulations due to precipitation intermittency changes, the central Greenland isotopic against temperature gradient differences is also driven by sea surface condition (precipitation source) changes. The overall tendency is for gradients, where substantial sea surface warming occurs north of Greenland (HadAM3 A1B and A2), to be about twice those where no substantial warming occurs (LMDZ4 CO2 $\times$ 2 and 4, and HadAM3 SeaIce).

5. What can we learn about the interpretation Greenland ice cores from these simulations?

Here we consider what is learned about the interpretation of ice core measurements from these results. Sections 4.2 to 4.5 indicate sea surface condition changes exert significant control over isotopes recorded in Greenland ice cores. With that in mind, here we first provide an overview of the agreement between sea surface condition observations, and our warmer simulations, for the last interglacial. Implications and possible future studies are then discussed.

5.1. Previous warmer than present day sea surface temperature and sea ice changes

The Turney and Jones (2010) compilation of sea surface temperature observations are shown in Fig. 10 (square symbols). These Turney and Jones (2010) observations support the idea that maximum last interglacial sea surface temperature anomalies were larger at higher latitudes (*e.g.* Leduc et al., 2010). Additionally, the available interglacial Arctic sea ice indicators (Table 2) suggest that the minimum last interglacial sea ice concentration and (or) extent was reduced compared to the present day (Fig. 10, round symbols).

Observations of last interglacial sea ice concentration or extent reductions are spare and are not quantitative. The two observations agree with all of the simulated warmer climate sea ice concentration reductions (Fig. 4 and 10). A more detailed comparison with the simulated results is not possible with these data. There are more Turney and Jones (2010) observations of maximum last interglacial sea surface temperature changes (Fig. 10). All of the available observations are over plotted on HadAM3 SRES A1B (Fig. 10a) and LMDZ4 CO2 $\times$ 4 (Fig. 10b) sea surface temperature changes. Fig. 10 shows that both sets of sea surface temperature changes agree with the broad pattern of observations, with larger maximum last interglacial sea surface temperature anomalies at higher latitudes. However, beyond this agreement, rather like the sea ice observations, there is a lack of last interglacial observations in critical regions particularly north of Greenland. HadAM3 and LMDZ4 sea surface changes are quite different in these regions. However a lack of sea surface temperature observations north of 72°N means these simulation differences cannot be assessed.

5.2. How could the interpretation last interglacial elevation and temperature changes from $\delta^{18}O$ be improved?

In addition to the last interglacial temperature reconstruction problem, there has been interest in whether isotopic ice core records can also be used to help reconstruct the elevation of past Greenland ice sheet core sites (Vinther et al., 2009; Masson-Delmotte et al., 2011). This would help with assessing the past and possible future impact of such changes on the ice sheet (*e.g.* Letreguilly et al., 1991; Cuffey and Marshall, 2000; Chen et al., 2006; Velicogna, 2009; van de Berg et al., 2011).

To aid these future interpretations of interglacial ice $\delta^{18}O$, isotopic modelling studies which use varying Greenland icesheet morphologies would be

very useful. Other changes which should also be examined include directly orbitally driven insolation effects. For example, radiation driven impacts on the hydrological cycle, and hence on Greenland $\delta^{18}O$ should be clarified (Masson-Delmotte et al., 2011). Interglacial vegetation growth associated with any reduction in the Greenland icesheet also likely has an impact on Greenland $\delta^{18}O$ (Schurgers et al., 2007; Masson-Delmotte et al., 2011). In addition to these possible single attribute modelling studies, fully coupled ocean-atmosphere-seaice-vegetation model studies would also be of value. For example, a reduced interglacial ice sheet could decrease ice core site elevations, increase Greenland vegetation, change local atmospheric circulation, and effect sea ice. Thus fully coupled model runs will also be necessary if we wish to achieve the best possible simulation of last interglacial isotopes across Greenland. However, in the meantime, it is likely that attribution studies focussing on single aspects of these problems may be especially helpful in terms of developing our understanding of the critical processes.

Finally we note that our findings suggest that the reconstruction of past interglacial ice sheet elevations will also require additional sea surface temperature constraints. These additional data would be very helpful in reducing the uncertainties on a joint interglacial reconstruction of temperature and elevation changes from $\delta^{18}O$.

6. Summary and conclusions

It is of considerable interest to the climate community to better understand isotopic ice core records from Greenland; particularly from the past warm interglacial maxima (around 125-130 ky). Five Greenland stable water isotope ice core records suggest that between the present day and the peak of the last warm interglacial, there was an increase in $\delta^{18}O$ of at least 3 ‰ in central and north-western Greenland. There were also likely increases in southern and eastern Greenland. The use of isotopically enabled general circulation models is therefore of value to the ice core and ice sheet community. With this in mind, two sets of isotopically enabled atmospheric general circulation model simulations, applying the HadAM3 and LMDZ4 models, were used to investigate warm climate changes (Sime et al., 2008, 2009b; Tindall et al., 2009; Risi et al., 2010). In both cases, warmer than present day simulations were generated by applying greenhouse gas forced patterns of sea surface temperature and sea ice change to the models (Sime et al., 2008; Masson-Delmotte et al., 2011). Because traditional orbitally driven simu-

lations show less than 20% of the observed $\delta^{18}O$ and temperature change, interpretation of the interglacial $\delta^{18}O$ rise from these traditional simulations is difficult. The greenhouse gas warmed approach is therefore a useful complement to the orbital approach, and has here highlighted a possible driver for the interglacial rise in Greenland $\delta^{18}O$.

In terms of the models, we have shown that the HadAM3 and LMDZ4 isotopic responses to sea surface condition changes are very similar (Appendix C), suggesting that any differences in inter-model physics are not a significant factor in our results. The central Greenland $\delta^{18}O$ changes for warmer HadAM3 simulations and for the warmest LMDZ4 simulation both show increases in $\delta^{18}O$ that are commensurate with the observed interglacial rise. A temperature increase of +4.7°C for HadAM3 is associated with a rise of 3.6 ‰ in $\delta^{18}O$. A temperature increase of +7.3°C for LMDZ4 is associated with a rise of 1.8 ‰ in $\delta^{18}O$. Our simulations show smaller changes in temperature, precipitation, $\delta^{18}O$, and d-excess in southern regions of Greenland, and larger changes in central eastern and northern regions of Greenland.

We find that understanding sea surface condition changes is key to understanding Greenland isotopic changes. This is largely because sea surface changes drive differences in precipitation sources, which affect $\delta^{18}O$ values over Greenland. Precipitation sourced from local high-latitude regions is enriched in $\delta^{18}O$. Increasing (decreasing) the proportion of locally source precipitation therefore raises (lowers) $\delta^{18}O$ in Greenland snow. For the HadAM3 warm climate simulations, evaporation changes tend to be strongly positive over the northerly areas around Greenland, due to the combined effect of reduced sea ice and strongly increased sea surface temperatures. This leads to substantially more local ($\delta^{18}O$ enriched) precipitation falling over northern Greenland. The LMDZ4 simulations feature stronger sea surface temperature increases south of 50°N and little change around Greenland. This leads to a higher proportion of warm climate ($\delta^{18}O$ depleted) distally sourced Greenland precipitation. For this reason, the LMDZ4 $\delta^{18}O$ changes over Greenland are much smaller than those in HadAM3, even when Greenland temperature increases are similar. These differences in HadAM3 and LMDZ4 sea surface temperature forcings lead the HadAM3 $\delta^{18}O$ against temperature gradients to be about twice the magnitude of LMDZ4 gradients. Given that during colder than present day climate periods, $\delta^{18}O$ was more likely sourced from distal (depleted) sources (Masson-Delmotte et al., 2005), a warm climate change towards more locally sourced vapour during the last interglacial may be more likely.

We show there are some non-linearities in the response of Greenland temperature and $\delta^{18}O$ to reductions in sea ice and sea surface temperature increases: applying changes in sea surface temperature or sea ice separately is not equivalent to applying both changes simultaneously. While $\delta^{18}O$ source effects explain the differences between the simulations, we also find that changes in precipitation intermittency explain large geographical differences in the relationship between $\delta^{18}O$ and temperature across Greenland.

The Turney and Jones (2010) last interglacial sea surface temperature change dataset lacks observations from around northern Greenland. This means that these observations do not tell us which of the sets of isotopic model simulation results better resembles last interglacial sea surface conditions. Both the HadAM3 and the LMDZ4 sets of sea surface temperature changes, and hence also precipitation source changes, agree with the broad pattern of last interglacial sea surface temperature information (Fig. 10). This means that neither set of simulation results can be definitely excluded as unrepresentative of last interglacial changes. This is problematic, in that it indicates that a very broad range of interglacial temperatures, across Greenland, could be in agreement with a > 3 ‰ increase in interglacial $\delta^{18}O$. In essence anywhere between 4 and >10 °C seems possible. Such a broad range of uncertainty also affects the ability to be able to interpret past interglacial changes in the elevation of the Greenland ice sheet: if significant sea surface warming took place around the northern edge of Greenland, simulation results imply that a reduced interglacial elevation of the central Greenland ice sheet surface may not be necessary to explain the isotopically enriched interglacial values. However, if this warming did not occur, larger elevation changes become more likely. Further isotopic modelling studies, which also examine the impact of ice sheet, vegetation, and insolation driven $\delta^{18}O$ impacts, would be of considerable value in addressing this question.

In conclusion, this study represents an original contribution to the debate regarding the drivers of isotope-temperature relationships. We have shown, for the first time, that if seas to the north of Greenland warm by around +4 to +6 °C, and sea ice is reduced, then central Greenland $\delta^{18}O$ rises of > 3 ‰ can be simulated at temperatures of +5°C. Additional marine core observations from northern Greenland, which help establish the magnitude of interglacial changes in sea surface conditions, alongside further modelling studies, will help in assessing whether a sea ice reduction is indeed the most likely cause of high interglacial $\delta^{18}O$ in Greenland ice cores.

Acknowledgements

This is Past4Future contribution no 22. The research leading to these results has received funding from the European Union's Seventh Framework programme (FP7/2007-2013) under grant agreement no 243908, the Agence Nationale de la Recherche NEEM and GREENLAND projects, and UK-NERC grant NE/J004804/1. It forms a part of the British Antarctic Survey Polar Science for Planet Earth Programme. The LMDZ4 simulations were run on the NEC-SX6 of the IDRIS computer center.

References

Adler, R.E., Polyak, L., Ortiz, J.D., Kaufman, D.S., Channell, J.E.T., Xuan, C., Grottoli, A.G., Selln, E., Crawford, K.A., 2009. Sediment record from the western Arctic Ocean with an improved Late Quaternary age resolution: HOTRAX core HLY0503-8JPC, Mendeleev Ridge. Global and Planetary Change 68, 18–29.

van de Berg, W.J., van den Broeke, M., Ettema, J., van Meijgaard, E., Kaspar, F., 2011. Significant contribution of insolation to Eemian melting of the Greenland ice sheet. Nature Geoscience 4, 679–683.

Burgess, E.W., Forster, R.R., Box, J.E., Mosley-Thompson, E., Bromwich, D.H., Bales, R.C., Smith, L.C., 2010. A spatially calibrated model of annual accumulation rate on the Greenland Ice Sheet (19582007). Journal of Geophysical Research 115, F02004+.

Burkhart, J.F., Hutterli, M., Bales, R.C., McConnell, J.R., 2004. Seasonal accumulation timing and preservation of nitrate in firn at Summit, Greenland. Journal of Geophysical Research 109, D19302+.

CAPE Project Members, 2006. Last Interglacial Arctic warmth confirms polar amplification of climate change. Quaternary Science Reviews 25, 1383 – 1400.

Capron, E., Landais, A., Chappellaz, J., Schilt, A., Buiron, D., Dahl-Jensen, D., Johnsen, S.J., Jouzel, J., Lemieux-Dudon, B., Loulergue, L., Leuenberger, M., Masson-Delmotte, V., Meyer, H., Oerter, H., Stenni, B., 2010. Millennial and sub-millennial scale climatic variations recorded in polar ice cores over the last glacial period. Climate of the Past 6, 345–365.

699 Chen, J.L., Wilson, C.R., Tapley, B.D., 2006. Satellite Gravity Measurements
700 Confirm Accelerated Melting of Greenland Ice Sheet. Science 313, 1958–
701 1960.

702 Colville, E.J., Carlson, A.E., Beard, B.L., Hatfield, R.G., Stoner, J.S., Reyes,
703 A.V., Ullman, D.J., 2011. Sr-Nd-pb isotope evidence for Ice-Sheet presence
704 on southern greenland during the last interglacial. Science 333, 620–623.

705 Cronin, T., Gemery, L., Jr., W.B., Jakobsson, M., Polyak, L., Brouwers],
706 E., 2010. Quaternary Sea-ice history in the Arctic Ocean based on a new
707 Ostracode sea-ice proxy. Quaternary Science Reviews 29, 3415 – 3429.
708 APEX: Arctic Palaeoclimate and its Extremes.

709 Cuffey, K., Clow, G., Alley, R., Stuiver, M., Waddington, E., Saltus, R.,
710 1995. Large Arctic temperature change at the Wisconsin-Holocene glacial
711 transition. Science 270, 455–458.

712 Cuffey, K., Paterson, W., 2010. The Physics of Glaciers, 4th Edition. Elsevier
713 Academic Press.

714 Cuffey, K.M., Marshall, S.J., 2000. Substantial contribution to sea-level rise
715 during the last interglacial from the Greenland ice sheet. Nature 404,
716 591–594.

717 Dahl-Jensen, D., Mosegaard, K., Gundestrup, N., Clow, G.D., Johnsen, S.J.,
718 Hansen, A.W., Balling, N., 1998. Past Temperatures Directly from the
719 Greenland Ice Sheet. Science 282, 268–271.

720 Dansgaard, W., 1964. Stable isotopes in precipitation. Tellus 16, 436–468.

721 Gordon, C., Cooper, C., Senior, C.A., Banks, H., Gregory, J.M., Johns, T.C.,
722 Mitchell, J.F.B., Wood, R.A., 2000. The simulation of SST, sea ice extents
723 and ocean heat transports in a version of the Hadley Centre coupled model
724 without flux adjustments. Climate Dynamics 16, 147–168.

725 Govin, A., Braconnot, P., Capron, E., Cortijo, E., Duplessy, J.C., Jansen,
726 E., Labeyrie, L., Landais, A., Marti, O., Michel, E., Mosquet, E., Rise-
727 brobakken, B., Swingedouw, D., Waelbroeck, C., 2012. Persistent influence
728 of ice sheet melting on high northern latitude climate during the early Last
729 Interglacial. Climate of the Past 8, 483–507.

730 GRIP Project Members, 1993. Climate instability during the last interglacial
731 period recorded in the GRIP ice core. Nature 364, 203–207.

732 Helsen, M., van de Wal, R., van den Broeke, M., 2007. The isotopic composi-
733 tion of present-day Antarctic snow in a Lagrangian atmospheric simulation.
734 Journal of Climate 20, 739–756.

735 Hoffmann, G., Heimann, M., 1997. Water isotope modeling in the Asian
736 monsoon region. Quaternary International 37, 115–128.

737 Hoffmann, G. Werner, M., Heimann, M., 1998. The Water Isotope Module of
738 the ECHAM Atmospheric General Circulation Model - A study on Time
739 Scales from Days to Several Years. Journal of Geophysical Research 103,
740 16871–16896.

741 Johnsen, S.J., Clausen, H.B., Cuffey, K.M., Schwander, J., Creyts, T., 2000.
742 Physics of Ice Core Records. Hokkaido University Press, Sapporo. volume
743 159. chapter Diffusion of stable isotopes in polar firn and ice: the isotope
744 effect in firn diffusion. pp. 121–140.

745 Johnsen, S.J., Dahl-Jensen, D., Dansgaard, W., Gundestrup, N., 1995.
746 Greenland palaeotemperatures derived from GRIP bore hole temperature
747 and ice core isotope profiles. Tellus B 47, 624–629.

748 Johnsen, S.J., Dahl-Jensen, D., Gundestrup, N., Steffensen, J.P., Clausen,
749 H.B., Miller, H., Masson-Delmotte, V., Sveinbjrnsdottir, A.E., White, J.,
750 2001. Oxygen isotope and palaeotemperature records from six Green-
751 land ice-core stations: Camp Century, Dye-3, GRIP, GISP2, Renland and
752 NorthGRIP. Journal of Quaternary Science 16, 299–307.

753 Johnsen, S.J., Dansgaard, W., Clausen, H.B., Langway, C.C., 1972. Oxygen
754 Isotope Profiles through the Antarctic and Greenland Ice Sheets. Nature
755 235, 429–434.

756 Jouzel, J., Alley, R.B., Cuffey, K.M., Dansgaard, W., Grootes, P., Hoffmann,
757 G., Johnsen, S.J., Koster, R.D., Peel, D., Shuman, C., Stievenard, M.,
758 Stuiver, M., White, J., 1997. Validity of the temperature reconstruction
759 from water isotopes in ice cores. Journal of Geophysical Research - Oceans
760 102, 26471–26487. 97JC01283.

761 Jouzel, J., Koster, R.D., Suozzo, R.J., Russell, G.L., 1994. Stable water
762 isotope behavior during the last glacial maximum: A general circulation
763 model analysis. Journal of Geophysical Research 99, 25791–25802.

764 Kobashi, T., Kawamura, K., Severinghaus, J.P., Barnola, J.M., Nakaegawa,
765 T., Vinther, B.M., Johnsen, S.J., Box, J.E., 2011. High variability of
766 Greenland surface temperature over the past 4000 years estimated from
767 trapped air in an ice core. Geophysical Research Letters 38, L21501.

768 Krinner, G., Genthon, C., Jouzel, J., 1997. GCM analysis of local influences
769 on ice core δ signals. Geophysical Research Letters 24, 2825–2828.

770 Krinner, G., Guicherd, B., Ox, K., Genthon, C., Magand, O., 2008. Influence
771 of oceanic boundary conditions in simulations of Antarctic climate and
772 surface mass balance change during the coming century. Journal of Climate
773 21, 938–962.

774 Krinner, G., Werner, M., 2003. Impact of precipitation seasonality changes
775 on isotopic signals in polar ice cores: a multi-model analysis. Earth and
776 Planetary Science Letters 4, 525–538.

777 Lachlan-Cope, T.A., Connolley, W.M., Turner, J., 2007. Effects of
778 tropical sea surface temperature (SST) errors on the Antarctic at-
779 mospheric circulation of HadCM3. Geophysical Research Letters 34.
780 Doi:10.1029/2006GL029067.

781 Landais, A., Chappellaz, J., Delmotte, M., Jouzel, J., Blunier, T., Bourg,
782 C., Caillon, N., Cherrier, S., Malaizé, B., Masson-Delmotte, V., Raynaud,
783 D., Schwander, J., Steffensen, J.P., 2003. A tentative reconstruction of
784 the last interglacial and glacial inception in Greenland based on new gas
785 measurements in the Greenland Ice Core Project (GRIP) ice core. Journal
786 of Geophysical Research 108, 4563+.

787 Landais, A., Masson-Delmotte, V., Jouzel, J., Raynaud, D., Johnsen, S., Hu-
788 ber, C., Leuenberger, M., Schwander, J., Minster, B., 2005. The glacial
789 inception as recorded in the NorthGRIP Greenland ice core: timing, struc-
790 ture and associated abrupt temperature changes. Climate Dynamics 26,
791 273–284.

792 Lang, N., Wolff, E.W., 2010. Interglacial and glacial variability from the
793 last 800 ka in marine, ice and terrestrial archives. Climate of the Past
794 Discussions 6, 2223–2266.

795 Langway, C., Oeschger, H., Dansgaard, W. (Eds.), 1985. Greenland ice core:
796 Geophysics, geochemistry and environment. volume Geophysical Mono-
797 graphs. American Geophysics Union, Washington D.C.

798 Leduc, G., Schneider, R., Kim, J.H., Lohmann, G., 2010. Holocene and
799 Eemian sea surface temperature trends as revealed by alkenone and Mg/Ca
800 paleothermometry. Quaternary Science Reviews 29, 989 – 1004.

801 Letreguilly, A., Reeh, N., Huybrechts, P., 1991. The Greenland ice sheet
802 through the last glacial-interglacial cycle. Global and Planetary Change
803 4, 385–394.

804 MARGO Project Members, 2009. Constraints on the magnitude and patterns
805 of ocean cooling at the last glacial maximum. Nature Geoscience 2, 127–
806 132.

807 Masson-Delmotte, V., Braconnot, P., Hoffmann, G., Jouzel, J., Kageyama,
808 M., Landais, A., Lejeune, Q., Risi, C., Sime, L., Sjolte, J., Swingedouw,
809 D., Vinther, B., 2011. Sensitivity of interglacial Greenland temperature
810 and δ^{18}O to orbital and CO_2 forcing: climate simulations and ice core data.
811 Climate of the Past Discussions 7, 1585–1630.

812 Masson-Delmotte, V., Buiron, D., Ekaykin, A., Frezzotti, M., Gallée, H.,
813 Jouzel, J., Krinner, G., Landais, A., Motoyama, H., Oerter, H., Pol, K.,
814 Pollard, D., Ritz, C., Schlosser, E., Sime, L.C., Sodemann, H., Stenni,
815 B., Uemura, R., Vimeux, F., 2010. A comparison of the present and
816 last interglacial periods in six Antarctic ice cores. Climate of the Past
817 Discussions 6, 2267–2333.

818 Masson-Delmotte, V., Dreyfus, G., Braconnot, P., Johnsen, S., Jouzel, J.,
819 Kageyama, M., Landais, A., Loutre, M.F., Nouet, J., Parrenin, F., Ray-
820 naud, D., Stenni, B., Tuenter, E., 2006. Past temperature reconstructions
821 from deep ice cores: relevance for future climate change. Climate of the
822 Past 2, 145–165.

823 Masson-Delmotte, V., Jouzel, J., Landais, A., Stievenard, M., Johnsen, S.J.,
824 White, J.W.C., Werner, M., Sveinbjornsdottir, A., Fuhrer, K., 2005. GRIP

825 Deuterium Excess Reveals Rapid and Orbital-Scale Changes in Greenland
826 Moisture Origin. Science 309, 118–121.

827 NGRIP Project Members, 2004. High-Resolution record of northern hemi-
828 sphere climate extending into the last interglacial period. Nature 431,
829 147–151.

830 Noone, D., 2008. The influence of midlatitude and tropical overturning circu-
831 lation on the isotopic composition of atmospheric water vapor and Antarc-
832 tic precipitation. Journal of Geophysical Research 113, D04102+.

833 Noone, D., Simmonds, I., 2004. Sea ice control of water isotope transport
834 to Antarctica and implications for ice core interpretation. Journal of Geo-
835 physical Research - Atmospheres 109, D07105+.

836 Noone, D., Sturm, C., 2010. Isoscapes: Understanding movement, patterns,
837 and process on Earth through isotope mapping. Springer. chapter Com-
838 prehensive dynamical models of global and regional water isotope distri-
839 butions. p. 487.

840 Nørgaard-Pedersen, N., Mikkelsen, N., Lassen, S.J., Kristoffersen, Y., Shel-
841 don, E., 2007. Reduced sea ice concentrations in the Arctic Ocean during
842 the last interglacial period revealed by sediment cores off northern Green-
843 land. Paleoceanography 22, PA1218+.

844 Otto-Bliesner, B.L., Marshall, S.J., Overpeck, J.T., Miller, G.H., Hu, A.,
845 members, C.L.I.P., 2006. Simulating Arctic Climate Warmth and Icefield
846 Retreat in the Last Interglaciation. Science 311, 1751–1753.

847 Pope, V.D., Gallani, M.L., Rowntree, P.R., Stratton, R.A., 2000. The im-
848 pact of new physical parametrizations in the Hadley Centre climate model:
849 HadAM3. Climate Dynamics 16, 123–146.

850 Rayner, N.A., Parker, D.E., Horton, E.B., Folland, C.K., Alexander, L.V.,
851 Rowell, D.P., Kent, E.C., Kaplan, A., 2003. Global analyses of sea sur-
852 face temperature, sea ice, and night marine air temperature since the late
853 nineteenth century. Journal of Geophysical Research 108, 4407+.

854 Risi, C., Bony, S., Vimeux, F., Jouzel, J., 2010. Water-stable isotopes in
855 the LMDZ4 general circulation model: Model evaluation for present-day

and past climates and applications to climatic interpretations of tropical isotopic records. Journal of Geophysical Research 115, D12118.

Schmidt, G.A., LeGrande, A.N., Hoffmann, G., 2007. Water isotope expressions of intrinsic and forced variability in a coupled ocean-atmosphere model. Journal of Geophysical Research D10103, –.

Schurgers, G., Mikolajewicz, U., Gröger, M., Maier-Reimer, E., Vizcaíno, M., Winguth, A., 2007. The effect of land surface changes on eemian climate. Climate Dynamics 29, 357–373.

Severinghaus, J.P., Brook, E.J., 1999. Abrupt climate change at the end of the last glacial period inferred from trapped air in polar ice. Science 286, 930–934.

Severinghaus, J.P., Sowers, T., Brook, E.J., Alley, R.B., Bender, M.L., 1998. Timing of abrupt climate change at the end of the Younger Dryas interval from thermally fractionated gases in polar ice. Nature 391, 141–146.

Sime, L.C., Lang, N., Thomas, E.R., Mulvaney, R., 2011. On high resolution sampling of short ice cores: Dating and temperature information recovery from Antarctic Peninsula virtual cores. Journal of Geophysical Research - Atmospheres 116, D20117.

Sime, L.C., Marshall, G.J., Mulvaney, R., Thomas, E.R., 2009a. Interpreting temperature information from ice cores along the Antarctic Peninsula: ERA40 analysis. Geophysical Research Letters 36, L18801.

Sime, L.C., Stevens, D.P., Heywood, K.J., Oliver, K.I.C., 2006. A Decomposition of the Atlantic Meridional Overturning. Journal of Physical Oceanography 36, 2253–2270.

Sime, L.C., Tindall, J., Wolff, E., Connolley, W., Valdes, P., 2008. The Antarctic isotopic thermometer during a CO2 forced warming event. Journal of Geophysical Research - Atmospheres D24119. Doi: 10.1029/2008JD010395.

Sime, L.C., Wolff, E.W., Oliver, K.I.C., Tindall, J.C., 2009b. Evidence for warmer interglacials in East Antarctic ice cores. Nature 462, 342–345.

886 Sjolte, J., Hoffmann, G., Johnsen, S.J., Vinther, B.M., Masson-Delmotte, V.,
887 Sturm, C., 2011. Modeling the water isotopes in Greenland precipitation
888 19592001 with the meso-scale model REMO-iso. Journal of Geophysical
889 Research 116, D18105.

890 Stroeve, J., Holland, M.M., Meier, W., Scambos, T., Serreze, M., 2007. Arctic
891 sea ice decline: Faster than forecast. Geophysical Research Letters 34,
892 L09501+.

893 Suwa, M., von Fischer, J.C., Bender, M.L., Landais, A., Brook, E.J., 2006.
894 Chronology reconstruction for the disturbed bottom section of the GISP2
895 and the GRIP ice cores: Implications for termination II in greenland.
896 Journal of Geophysical Research 111, D02101+.

897 Svensson, A., Andersen, K.K., Bigler, M., Clausen, H.B., Dahl-Jensen, D.,
898 Davies, S.M., Johnsen, S.J., Muscheler, R., Parrenin, F., Rasmussen, S.O.,
899 Röthlisberger, R., Seierstad, I., Steffensen, J.P., Vinther, B.M., 2008. A
900 60 000 year Greenland stratigraphic ice core chronology. Climate of the
901 Past 4, 47–57.

902 Tindall, J.C., Valdes, P.J., Sime, L.C., 2009. Stable water isotopes in
903 HadCM3: Isotopic signature of El Niño Southern Oscillation and the trop-
904 ical amount effect. Journal of Geophysical Research 114, D04111.

905 Turney, C.S., Jones, R.T., 2010. Does the Agulhas Current amplify global
906 temperatures during super-interglacials? Journal of Quaternary Science
907 25, 839–843.

908 Velicogna, I., 2009. Increasing rates of ice mass loss from the Greenland and
909 Antarctic ice sheets revealed by GRACE. Geophysical Research Letters
910 36, L19503.

911 Vinther, B., Jones, P., Briffa, K., Clausen, H., Andersen, K., Dahl-Jensen,
912 D., Johnsen, S., 2010. Climatic signals in multiple highly resolved stable
913 isotope records from Greenland. Quaternary Science Reviews 29, 522 –
914 538.

915 Vinther, B.M., Buchardt, S.L., Clausen, H.B., Dahl-Jensen, D., Johnsen,
916 S.J., Fisher, D.A., Koerner, R.M., Raynaud, D., Lipenkov, V., Andersen,
917 K.K., Blunier, T., Rasmussen, S.O., Steffensen, J.P., Svensson, A.M., 2009.
918 Holocene thinning of the Greenland ice sheet. Nature 461, 385–388.

Watson, A.J., Naveira Garabato, A.C., 2006. The role of southern ocean mixing and upwelling in glacial-interglacial atmospheric co2 change. Tellus Series B Chemical And Physical Meteorology 58, 73–87.

Werner, M., Heimann, M., 2002. Modeling interannual variability of water isotopes in Greenland and Antarctica. Journal of Geophysical Research D - Atmospheres 107.

Werner, M., Langebroek, P.M., Carlsen, T., Herold, M., Lohmann, G., 2011. Stable water isotopes in the ECHAM5 general circulation model: Toward high-resolution isotope modeling on a global scale. Journal of Geophysical Research 116, D15109+.

Werner, M., Mikolajewicz, U., Heimann, M., Hoffmann, G., 2000. Borehole versus isotope temperatures on Greenland: Seasonality does matter. Geophysical Research Letters 27, 723–726.

Wunsch, C., 2003. Determining paleoceanographic circulations, with emphasis on the last glacial maximum. Quaternary Science Reviews 22, 371 – 385.

Table 1: Simulation sea surface condition (SSC) and atmospheric gas boundary conditions. Simulations are run for 20 or more years.

Experiment	Applied SSC anomaly		HadCM3 and IPSL atmosphere		
	SST	Sea ice	CO_2 $ppmv$[a]	N_2O $ppbv$[b]	CH_4 $ppmv$
Present day HadAM3 [c]	HadISST	HadISST	353	310	1.72
Present day LMDZ4 [d]	AMIP[e]	AMIP	348	306	1.65
Warm HadAM3 (SRES A1B)	HadCM3	HadCM3	720	370	2.0
Very warm HadAM3 (SRES A2)	HadCM3	HadCM3	820	370	2.0
Warm LMDZ4 (CO2 x 2)	IPSL	IPSL	696	306	1.65
Very warm LMDZ4 (CO2 x 4)	IPSL	IPSL	1392	306	1.65
SST HadAM3 (SRES A1B)	HadCM3	HadISST	720	370	2.0
SeaIce HadAM3 (SRES A1B)	HadISST	HadCM3	720	370	2.0

[a] *ppmv* - parts per million by volume. [b] *ppbv* - parts per billion by volume. [c] Present-day centered on 1990.

[d] Present-day centered on 1992. [e] Atmospheric Model Intercomparison Project. See text for further details.

Table 2: Compilation of observations of Northern Hemisphere sea ice change for warmer interglacial conditions.

Site Name	**Latitude** °N [deg.min]	**Longitude** °W [deg.min]	**Water depth** [m]	**Time** MIS or ky	**Proxy**	**Evaluation**
GreenICE (c11)	84.49	74.16	1089	MIS5e-present (approx 128-0 ky)	Subpolar forams	Reduced sea ice in MIS 5a compared to present suggestion about season
NP26-5/32	78.59	178.09	1435	130-0 ky	Ostracodes	Pattern similar to Holo indicator missing in ear (peak) interglacial, and at moderate levels later
Oden96/12-1pc	87.05	144.46	1003	240-0 ky	Ostracodes	Pattern similar to Holo indicator missing in ear (peak) interglacial, and at moderate levels later
PS2200-5	85.19	14.00	1073	240-0 ky	Ostracodes	Pattern similar to Holo indicator missing in ear (peak) interglacial, and at moderate levels later
PS1243	69.23	6.32	2710	240-0 ky	Ostracodes	Indicator absent in 5E
M23214	53.32	20.17	2119	196-0 ky	Ostracodes	Indicator absent in 5E
HLY0503-8JPC	79.36	172.30	2792	MIS7-1 (approx 250-0 ky)	Subpolar forams	Reduced sea ice in MIS 5a compared to present Suggests seasonally ice-

Table 3: Annual mean present day (and warmer climate) simulation results (and anomalies) for central Greenland (> 1300 m). Temperature, precipitation, $\delta^{18}O$, and temporal $\delta^{18}O$ against temperature gradients, as specified.

Experiment	Temperature °C	Precipitation kg m^2 yr^{-1} (%)	$\delta^{18}O$ ‰	gradient ‰ per °C
		Present day simulation results		
HadAM3 present day	−24.0	325.8	−23.9	
LMDZ4 present day	−18.8	454.0	−28.3	
		Warmer simulation anomalies		
HadAM3 SRES A1B	+4.7	+92.8 (+28.5)	+3.6	0.76
HadAM3 SRES A2	+5.4	+117.1 (+35.9)	+3.9	0.71
LMDZ4 CO2 x 2	+3.3	+74.1 (+16.4)	+0.31	0.09
LMDZ4 CO2 x 4	+7.3	+176.1 (+38.8)	+1.79	0.25
HadAM3 SRES A1B SST	+3.4	+57.9 (+17.8)	+2.1	0.63
HadAM3 SRES A1B SeaIce	+0.84	+21.5 (+6.6)	+0.25	0.29

Table 4: The percentage of simulated present day central Greenland precipitation which is sourced from different regions, and the mean $\delta^{18}O$ precipitation value associated with each source region.

Precipitation source region	HadAM3 precipitation (%)	LMDZ4 precipitation (%)	HadAM3 $\delta^{18}O$ in precipitation (‰)	LMDZ4 $\delta^{18}O$ in precipitation (‰)
High latitude	18	20	+5.1	+2.0
Mid-low latitude	51	51	−37.1	−38.2
Continental	31	29	−29.6	−29.2

Figure 1: Ice cores across Greenland which may feature some last interglacial ice, and maximum difference between present day (0-3 ky) and maximum 'last interglacial' values. Map (a) shows the sites of the ice cores, where possible $\delta^{18}O$ last interglacial records are available. Numbers next to the core sites indicate the difference between the present day (0 - 3 ky) $\delta^{18}O$ and the maximum (before 100 ky) ice core $\delta^{18}O$ values. The present day to 'maximum $\delta^{18}O$ values' given on map (a) have question marks or $>$ marks to indicate the available values are questionable or likely underestimates of true peak last interglacial differences. For visual simplicity, we have placed the isotopically lightest near bed Renland ice ($\delta^{18}O$ value of about -24 ‰, true age not known) at 123 ky (circled). It is likely that this also does not represent peak interglacial values.

Figure 2: Comparison between HadAM3 present day simulated and observed (see Appendix B) Greenland values. Shading shows the mean simulation (20 year average) (a) surface temperature (°C), (b) precipitation (kg m^{-2} yr^{-1}) , (c) $\delta^{18}O$ (‰), (d) δD (‰), (e) deuterium excess (anomalies relative to Greenland average), and (f) orography (m). The square symbols on each panel give equivalent observed values as detailed in Table 2. For easy of comparison simulation results are presented after linear interpolation onto a 50 km $\times$ 50 km equal area grid (Sime et al., 2008).

Figure 3: As Fig. 2 but for LMDZ4 present day simulation. Shading shows (a) surface temperature (°C), (b) precipitation (kg m^{-2} yr^{-1}), (c) $\delta^{18}O$ (‰), (d) δD (‰), (e) deuterium excess (anomalies relative to Greenland average), and (f) orography (m). The square symbols on each panels give equivalent observed values as detailed in Table B.2.

Figure 4: Differences between the present day and warmer simulation climatic and isotopic results. (a,b) HadAM3 SRES A1B simulation; (c,d) HadAM3 SRES A2 simulation; (e,f) LMDZ4 CO2 x 2; and (g,h) LMDZ4 CO2 x 4. Left hand panels (a,c,e,g) shading (and contouring) over Greenland shows the difference between the present day and individual simulation values of $\delta^{18}O$ (and surface temperature) values, shading over the ocean areas shows anomalous sea ice concentrations. Right hand panel (b,d,f,h) shading (and contouring) over Greenland shows the difference between the present day and individual sensitivity simulation values of d-excess (and precipitation changes, in percentage) values, shading over the ocean areas shows anomalous sea surface temperatures. In each case, the shading over the ocean areas show the forcing applied to the atmospheric model, whilst over Greenland the shading (and contouring) shows the model response to the boundary condition changes.

Figure 5: Changes in central Greenland seasonality between the HadAM3 SRES A1B and present day simulation, and the LMDZ4 CO2 x 4 and present day simulation. Panel (a) shows the HadAM3 model response over Greenland for mean monthly central Greenland ($>$ 1300 m) anomalous temperature (K), $\delta^{18}O$ (‰), precipitation (kg m^{-2} yr^{-1}), and d-excess. Panel (b) shows results for LMDZ4.

Figure 6: Changes in ocean and sea ice surface seasonality between the HadAM3 SRES A1B and present day simulation, and the LMDZ4 CO2 x 4 and present day simulation. Panel (a) shows HadAM3 changes in: Atlantic north of 70°N sea surface temperature (solid line); North Atlantic north of 45°N sea surface temperature changes (dashed line); North Atlantic sea ice area changes (solid line); Northern Hemisphere sea ice area changes (dashed line); Atlantic all north of 70°N evaporation changes (solid line); North Atlantic all north of 45°N evaporation changes (dashed line). Panel (b) shows similar changes for the LMDZ4 results. All solid (dashed) results are on the left (right) axis.

Figure 7: HadAM3 sensitivity simulation results. (a,b) HadAM3 SRES A1B SST simulation; (c,d) HadAM3 SRES A1B SeaIce simulation; (e,f) effects of SST and SeaIce simulation results added together. Left hand panels (a,c,e) shading (and contouring) over Greenland shows the difference between the present day and individual simulation values of $\delta^{18}O$ ‰ (and surface temperature °C) values, shading over the ocean areas shows anomalous ice concentrations. Right hand panel (b,d,f) shading (and contouring) over Greenland shows the difference between the present day and individual sensitivity simulation values of d-excess (and precipitation changes, in percentage) values, shading over the ocean areas shows anomalous sea surface temperatures.

Figure 8: Changes in the amount of precipitation sourced from high-latitude (local) regions between the present day and individual simulation results: (a) HadAM3 SRES A1B and (b) LMDZ4 CO2 $\times$ 4. Note that any reduction in the high-latitude sourced percentage means that an equivalent rise in the proportion of mid-low latitude and continentally sourced precipitation vapour is required to balance the budget.

Figure 9: Shading shows the $\delta^{18}O$ against temperature gradient (‰ per °C) between the present day and individual simulation results. (a) HadAM3 SRES A1B; (b) HadAM3 SRES A2; (c) LMDZ4 CO2 $\times$ 2; (d) LMDZ4 CO2 $\times$ 4; (e) HadAM3 SRES A1B SST; and (d) HadAM3 SRES A1B SeaIce. The contouring for the HadAM3 results shows the temperature biasing (K) changes (cannot be calculated for LMDZ4 results because necessary variables not available).

Figure 10: Observations of last interglacial sea surface temperature (K) and sea ice anomalies plotted over the top of (a) HadAM3 SRES A1B and (b) LMDZ4 CO2 $\times$ 4 sea surface temperature changes (K).

Appendix A. Further details on the isotopic simulations:

The HadAM3 present day boundary conditions are based on a monthly average of 1980-1999 HadISST sea surface temperature and sea-ice data (Rayner et al., 2003; Sime et al., 2008). The level of atmospheric CO_2 for the present day run is 353 ppmv. The LMDZ4 present day run uses very similar standards, using a monthly average of the sea surface condition observational record from 1978-2007, and a level of atmospheric CO_2 of 348 ppm.

The approach used to generate the warmer than present day simulations in the two AGCMs is very similar. Coupled ocean-atmosphere versions (HadCM3 and IPSL), of the respective AGCM are used to simulate warmer than present day climates. The sea surface temperature anomalies from each coupled model simulation are then applied to the present day simulation (Sime et al., 2008; Masson-Delmotte et al., 2011). The use of anomalies reduces the impact of known model errors. Both the HadCM3 and the IPSL model sea surface temperature outputs have regional biases compared with the observed present day sea surface temperature (Lachlan-Cope et al., 2007). These biases can affect the modelled climatology. However, by applying the HadCM3 and IPSL sea surface temperature fields as anomalies to the present day sea surface temperature boundary conditions, the effect of these biases is minimised (*e.g.* Krinner et al., 2008). Please see also Sime et al. (2008), Risi et al. (2010), and Masson-Delmotte et al. (2011) for additional background details.

For the HadAM3 warmer simulations the sea surface condition anomalies are obtained from the HadCM3 World Climate Research Programme's Coupled Model Inter-comparison Project phase 3 simulations. These simulations use the ocean-atmosphere coupled HadCM3 model (Gordon et al., 2000; Sime et al., 2006). The CO_2 and other atmospheric composition is based on Special Report on Emissions Scenarios (SRES) A1B and A2 experiments (see Table 1 for values), in each case focussed on the year 2100. The LMDZ4 warmer than present day simulations used here are very similar to to the HadAM3 simulations. The boundary conditions are also based on GHG driven (Table 1) IPSL simulation sea surface condition anomalies (Masson-Delmotte et al., 2011). Two additional isotopic HadAM3 sensitivity experiments individually simulate the effect of the SRES A1B warmer sea surface temperatures (SST) and the SRES A1B sea ice changes (SeaIce). All simulations use fixed (present day) Greenland ice sheet elevations. Please see Table 1 for a summary of the simulations.

Appendix B. Evaluation of the present day model simulations against observations:

Appendix B.1. Mean annual results:

Present day observations from the surface of the Greenland ice sheet were provided by Vinther et al. (2010) and Sjolte et al. (2011). Table B.3 provides a mean of these Table B.2 observations and the equivalent mean simulation values, using co-located model results. See also main text Table 3 and summary results, for the alternative simulation results using the Masson-Delmotte et al. (2011) definition of central Greenland *i.e.* using all points higher than 1300 m. The available observations (Table B.2) suggest that the HadAM3 present day simulation temperature is on average, 1.9°C warmer than the available observational values. For LMDZ4, the average temperature is 9.1°C too warm. Note, available observational sites are not equally representative of the whole of central Greenland. Whilst this unequal representation effect is minimised by our comparison through co-location of our model outputs, the comparison nevertheless is more representative of the central cold region (see also Fig. 2a and 3a for the position of the available observations).

The simulated annual mean precipitation values compare reasonably well with the available accumulation observations. Note, as with temperature, the observations are mainly representative of the highest, coldest, and driest region. The HadAM3 simulation is 4.8 kg m^{-2} yr^{-1} , or 26%, too dry compared with these available observations, and the LMDZ4 simulation is 8.12 kg m^{-2} yr^{-1}, or 44%, too wet. The wetter than observed LMDZ4 results are likely related to the warmer than observed simulated temperatures. For both HadAM3 and LMDZ4 the overall geographical pattern of the observations and simulation results compare quite well (Fig. 2b and 3b) although comparison with additional observational evidence (*e.g.* Burgess et al., 2010) suggests that, in common with other models (Sjolte et al., 2011), simulated southern Greenland precipitation is likely too high.

The annual mean isotopic values of the precipitation, in each simulation, are heavier than the observations (see also Fig. 2c and 3c). For HadAM3, comparison with the available observations suggests the HadAM3 simulation may on average be 8.6 ‰ too heavy, whilst LMDZ4 is closer to observations at 3.9 ‰ too heavy. The δD results follow a very similar pattern (see also Fig. 2d and 3d). This model-observation isotopic offset, particularly for HadAM3, seems too large to be simply explained by the warmer than

observed model temperatures. The orographic representation of Greenland is reasonable accurate for central regions (Fig. 2f) and precipitation amount is generally reasonable, thus there seems no obvious reason in the mean annual results for the isotopic offset. Some similar heavy $\delta^{18}O$ biases also appear also be present in some other models (*e.g.* Hoffmann and Heimann, 1998; Sjolte et al., 2011). For HadAM3, and perhaps also other models, one possibility to explain the model-observation different is that the seasonal representation of isotopes in precipitation is not accurate.

Appendix B.1.1. Seasonal results:

Danish Meteorological Institute (DMI) station observations (see Fig. B.11, for station positions) of monthly temperature provide a useful resource for checking monthly simulated temperatures. The monthly station observations are available over different observation periods. In some cases, the records are also split into more than one series: in these cases, the original series are treated as separate observational sets. Fig. B.12 shows the mean of each of these DMI observational records, with a standard deviation envelope (of $\pm$ 2 standard deviations to each side of the mean) in black and grey. Plotted over the top are results from the present HadAM3 (red) and LMDZ4 (blue) simulations, in each case co-located with the observed record.

The results show that the seasonality of the temperature cycle in each model is generally reasonable, with the maximum and minimum monthly model-observation temperatures co-incident or within a month at the majority of the sites. Most of the DMI observation sites are situated close to the coast, and are thus less useful for a more detailed evaluation the simulation performance over the central Greenland region. However the latter panels show results from Summit and Dye 2/3 sites (Fig. B.12). These tend to suggest that the simulated seasonal cycle of temperature, over central Greenland, is too warm and the amplitude is too small in LMDZ4, whilst in HadAM3 the amplitude may be a little too large (as suggested in Section 3.1). For the more coastal sites, there is more variety in the relationship between the observed and simulated results. This is at least partly due to the HadAM3 and LMDZ4 model resolution, which is too coarse to give a good representation of the complex coastline and topography.

The seasonality of central Greenland precipitation for HadAM3 looks reasonable in comparison with the available observational records: both HadAM3 and the Burkhart et al. (2004) observations for Greenland Summit also show a single August-September peak in accumulation. The LMDZ4

precipitation seasonality is less uni-modal, which agrees less well with the Burkhart et al. (2004) precipitation seasonality observations.

Fig. B.13 shows the present day precipitation and $\delta^{18}O$ seasonality for HadAM3, LMDZ4, and observational records (Sjolte et al., 2011). In each case, the top 20 years of each core was used to obtain the mean seasonal amplitude. Although similar model and observation methods were used for averaging the summer and winter values, the simulated HadAM3 summer $\delta^{18}O$ values seem to be 8.9 ‰ too enriched, whilst the winter values seem to be 5.6 ‰ too enriched compared with the observations. This affects the average annual offset (of 8.6 ‰ too heavy). The summer offset has a more dominant effect on the annual mean due to the larger amount of simulated HadAM3 summertime precipitation (Fig. B.13c). Additionally, the simulated 3.4 ‰ seasonal $\delta^{18}O$ amplitude is too large, as likely is the seasonal temperature amplitude. However, difficulties in accurately dating (*e.g.* Sime et al., 2011), and back diffusing the isotopic results, may reduce the amplitude of the core seasonal $\delta^{18}O$ amplitude, compared to its original amplitude (Johnsen et al., 2000; Vinther et al., 2010). This may partly explain the discrepancy between the simulated HadAM3 and observed ice core seasonal $\delta^{18}O$ amplitude. For LMDZ4, the summer $\delta^{18}O$ values are 2.2 ‰ too enriched, whilst the winter values are 4.4 ‰ too enriched, compared with observations. This leads to an average annual offset which is 3.9 ‰ too heavy. Unlike HadAM3, LMDZ4 precipitation is less seasonal, so the offset is not strongly dominated by the summer precipitation. The simulated seasonal $\delta^{18}O$ amplitude for LMDZ4 is on average 2.2 ‰. In percentage terms, the LMDZ4 simulation of the $\delta^{18}O$ cycle amplitude is 41% of the observed amplitude, whereas the HadAM3 cycle is 190% of the observed amplitude.

Table B.5: Greenland observations of temperature, accumulation, $\delta^{18}O$. The observations were compiled by Vinther et al. (2010); Sjolte et al. (2011) and by Valerie Masson-Delmotte.

Longitude °W	Latitude °N	Temperature °C	Accumulation kg m^2 yr^{-1}	$\delta^{18}O$ ‰
37.65	73.03	-	14.10	-36.75
37.63	73.94	-	11.70	-37.08
37.63	74.85	-32.20	10.60	-37.4
36.40	75.72	-32.90	10.49	-36.66
36.40	76.62	-	11.40	-36.68
36.39	77.52	-31.00	11.83	-35.6
37.95	79.23	-	9.75	-34.9
41.14	80.00	-	10.22	-33.65
37.65	73.03	-	17.17	-36.49
37.65	73.50	-32.30	15.52	-38.18
37.63	73.94	-	13.75	-38.97
37.63	74.40	-32.70	13.32	-36.68
37.63	74.85	-32.20	12.64	-38.27
37.63	75.25	-	11.00	-36.93
37.21	75.25	-	14.11	-39.59
36.91	75.28	-	11.58	-36.19
36.39	75.50	-32.60	11.69	-36.42
39.54	75.57	-	11.66	-36.39
36.33	75.65	-	12.90	-37.23
36.40	75.72	-32.90	13.59	-36.87
36.40	76.17	-	13.12	-38.44
36.40	76.62	-	10.45	-34.94
37.37	76.62	-	11.47	-36.20
34.46	76.62	-	14.81	-36.02
36.40	77.07	-31.10	12.38	-36.83
36.39	77.52	-31.00	11.01	-35.02
36.40	78.00	-30.90	13.27	-34.7
36.44	78.42	-	11.50	-32.63
36.50	78.83	-	10.83	-34.86
37.95	79.23	-	9.75	-34.72
39.51	79.62	-	11.30	-35.51
41.14	80.00	-	12.01	-35.45
41.13	80.36	-	13.08	-32.64
37.63	73.94	-	12.28	-37.29
36.40	76.62	-	10.98	-37.04
41.14	80.00	-	10.40	-33.87
37.63	73.94	-	12.25	-37.32
36.40	76.62	-	10.40	-36.46
41.14	80.00	-	10.17	-34.47
37.63	73.94	-	14.20	-37.14
36.40	76.62	-	9.90	-36.67

Table B.2: Continued table.

Longitude °W	Latitude °N	Temperature °C	Accumulation kg m^2 yr^{-1}	$\delta^{18}O$ ‰
68.83	76.52	-11.60	-	-24.17
16.67	81.60	-17.28	-	-25.15
48.12	61.22	1.200	-	-11.98
18.40	76.46	-11.90	-	-18.54
22.00	70.50	-7.59	-	-13.78
43.07	60.08	0.73	-	-9.76
43.83	65.18	-	56.00	-27.40
44.50	70.30	-	54.00	-28.87
37.32	71.12	-	28.90	-34.18
35.82	70.63	-	29.20	-33.08
37.48	70.65	-	30.60	-33.50
39.62	70.64	-	35.40	-32.51
35.85	71.76	-	21.50	-35.61
35.84	71.15	-	24.90	-34.83
26.73	71.27	-	50.00	-27.23
37.64	72.58	-	23.00	-35.10

Table B.3: Observational and simulation averages. Mean of available Table B.2 observations (see Fig. 2 and B.13 for locations) and co-located simulation results.

Obs / Experiment	Temperature	Accumulation	$\delta^{18}O$		
			annual	summer	winter
	°C	kg m^2 yr^{-1}	‰	‰	‰
Observations (Table B.2)	-32.0	18.3	-33.1	-29.4	-35.4
HadAM3 Present day	-30.0	21.6	-26.8	-20.4	-27.5
LMDZ4 Present day	-22.8	26.4	-27.5	-26.2	-31.5
HadAM3 SRES A1B	-24.4	30.7	-22.8	-18.3	-24.7
HadAM3 SRES A2	-23.5	33.5	-22.2	-18.2	-24.2
LMDZ4 CO2 x 2	-19.5	32.1	-28.4	-26.9	-30.5
LMDZ4 CO2 x 4	-15.1	41.2	-27.5	-26.2	-28.4
HadAM3 SRES A1B SST	-26.0	26.4	-24.2	-18.9	-26.0
HadAM3 SRES A1B SeaIce	-28.6	24.5	-26.6	-21.0	-27.0

Figure B.11: The location of DMI (Danish Meteorological Institute) observational sites.

Figure B.12: DMI monthly mean temperatures (black) and equivalent simulated HadAM3 (red) and LMDZ4 (blue) results. See Fig. B.11 for the location of the DMI observational stations. Grey envelope shows ± 2 standard deviations to each side of the observed mean. Length of records are shown in individual panel labels.

Figure B.13: The seasonality of the HadAM3 and LMDZ4 present day simulations. Panel (a) shows the HadAM3 summer minus winter simulation $\delta^{18}O$ (‰) seasonality (shaded) with similar core site seasonality observations (Vinther et al., 2010; Sjolte et al., 2011) overlain using shaded squares. Panel (b) shows similar results for the LMDZ4 present day simulation. Note that for clarity the colorbars are rescaled between the two simulations. (c) Lines show the mean monthly central Greenland ($>$ 1300 m) values for the present day HadAM3 (solid lines) and LMDZ4 (dashed line) simulation of temperature, $\delta^{18}O$, precipitation, and d-excess.

Appendix C. Checking model dependence: Do the models HadAM3 and LMDZ4 give similar results?

In order to check the sensitivity of results to the inter-model atmospheric physics, two original HadAM3 experiments are repeated using LMDZ4. Sea surface boundary conditions identical to the HadAM3 present day and HadAM3 SRES A1B experiments (Table 1) are applied to LMDZ4: in each case, the LMDZ4 experiments are run using the HadAM3 boundary condition files. This is useful because it allows us to check for impacts of physical differences between the LMDZ4 and HadAM3 models. Computational restrictions mean that these additional experiments are run for three years.

Comparing Fig. C.14a to Fig. 4a for LMDZ4 versus HadAM3, allows an inter-atmospheric model check of the temperature and $\delta^{18}O$ changes. The identical LMDZ4 and HadAM3 experiments show a similar pattern of warming and $\delta^{18}O$ enrichment. This indicates that the sea surface temperature changes are the main driver of the Greenland climate and isotopic changes, rather than inter-model difference in atmospheric or isotopic physics. It also provides additional evidence that it is these sea surface condition changes (rather than any inter-model physics differences) which lead uncertainties in interpreting past Greenland $\delta^{18}O$ changes in terms of temperature shifts. This is confirmed by Fig. C.14b, which shows the $\delta^{18}O$ against temperature gradient (‰ per °C) between the same additional LMDZ4 simulations. Like the HadAM3 equivalent Fig. 9a gradient results, much higher gradients across Greenland arise when LMDZ4 is forced by the larger HadCM3 A1B local sea surface warming to the north and east of Greenland. Additionally, the match between the contouring and shading on Fig. C.14b confirms that, like HadAM3, precipitation-temperature biasing changes drive most of the LMDZ4 smaller-scale geographical variability in the temporal $\delta^{18}O$ against temperature gradient.

Table C.4: Additional duplicate and water tagged simulations performed using LMDZ4

Isotopic model	Experiment	Applied SSC anomaly		CO_2	Water tagging	Length
		SST	Sea ice	$[ppmv^a]$		$[years]$
LMDZ4	Present day[b]	HadISST	HadISST	353	YES	3
LMDZ4	Present day[c]	AMIP[d]	AMIP	348	YES	3
LMDZ4	SRES A1B	HadCM3	HadCM3	720	YES	3
LMDZ4	CO2 x 4	IPSL	IPSL	1392	YES	3

[a] $ppmv$ - parts per million by volume. [b] Present-day centered on 1990. [c] Present-day centered on 1992.

[d] Atmospheric Model Intercomparison Project. See text for further details.

Figure C.14: Differences between the present day and SRES A1B simulations by LMDZ4 climatic and isotopic results. (a) Shading (and contouring) over Greenland shows the difference between the present day and warmer simulation values of $\delta^{18}O$ (and surface temperature) values. (b) Shading shows the $\delta^{18}O$ against temperature gradient (‰ per °C) between the present day and LMDZ4 SRES A1B warmer simulation results. Contouring shows the temperature biasing (K) changes.

Appendix D. Source tracking simulations

In order to examine the question of precipitation sources, the same experiments outlined in Appendix C above, were run using the LMDZ4 source-tracking feature. Please see Risi et al. (2010), and references therein for additional details. (Note no source-tracking feature is available for HadAM3.) Using source tracking is quite computationally intensive so three years of output is used. Table 4 shows the central Greenland $\delta^{18}O$ values for the two versions of the present day simulations. Fig. D.15 shows the same results, but for across the whole of Greenland, rather than for a single central Greenland average.

Figure D.15: Shading shows the mean annual $\delta^{18}O$ precipitation value associated with a given source, and contours show the percentage of precipitation associated with that particular source. Results are from the two present day experiments (left panels) HadAM3 present-day, and (right panels) LMDZ4 present day. Source regions are: (a,b) all sourced regions; no precipitation contours given because all values are 100%; (c,d) high-latitude (north of 50°N) sea surface areas, (e,f) mid-low latitude (south of 50°N) sea surface areas, and (g,h) continental (all non-sea surface).

*Figure
Click here to download high resolution image

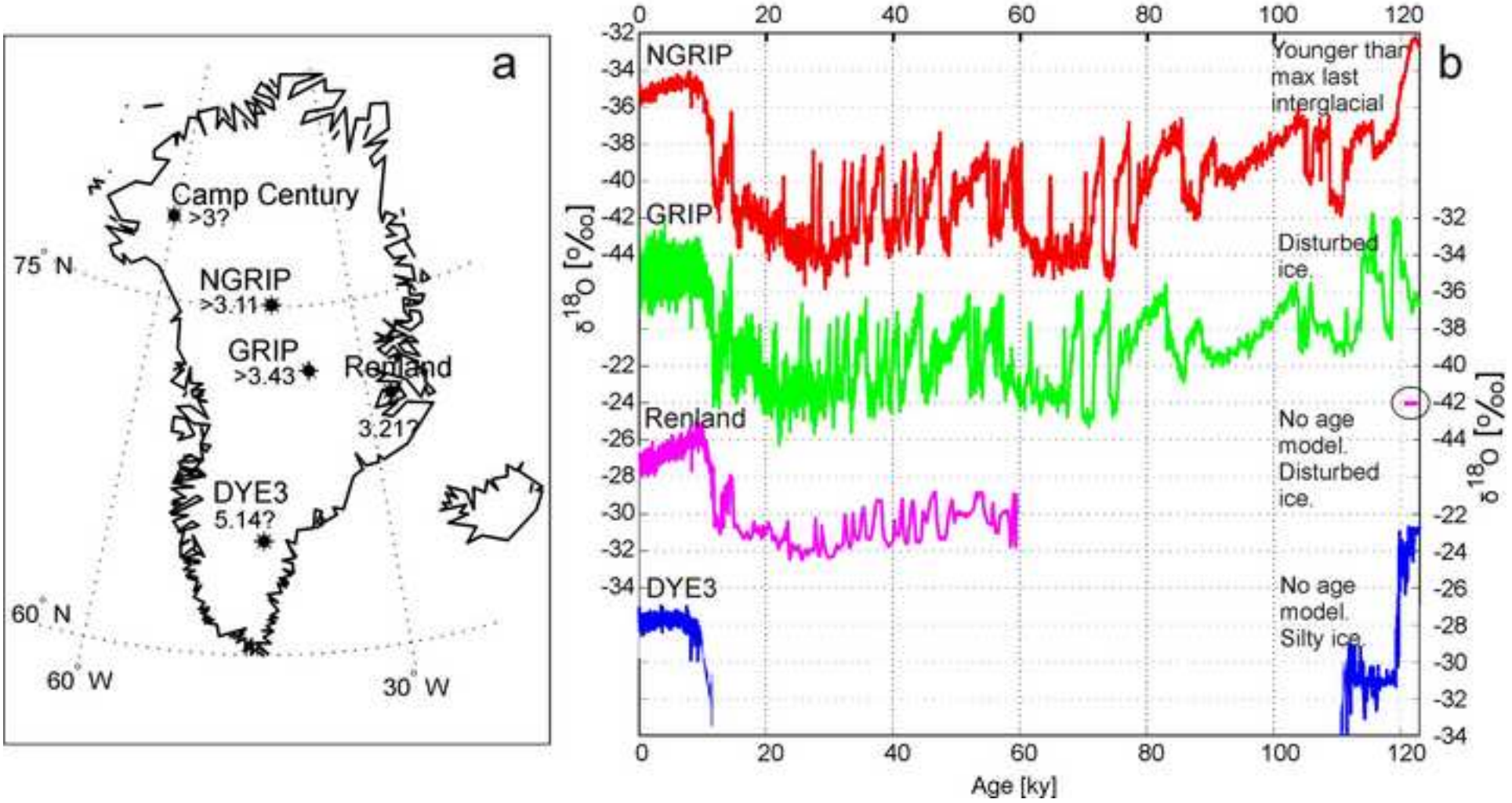

*Figure
Click here to download high resolution image

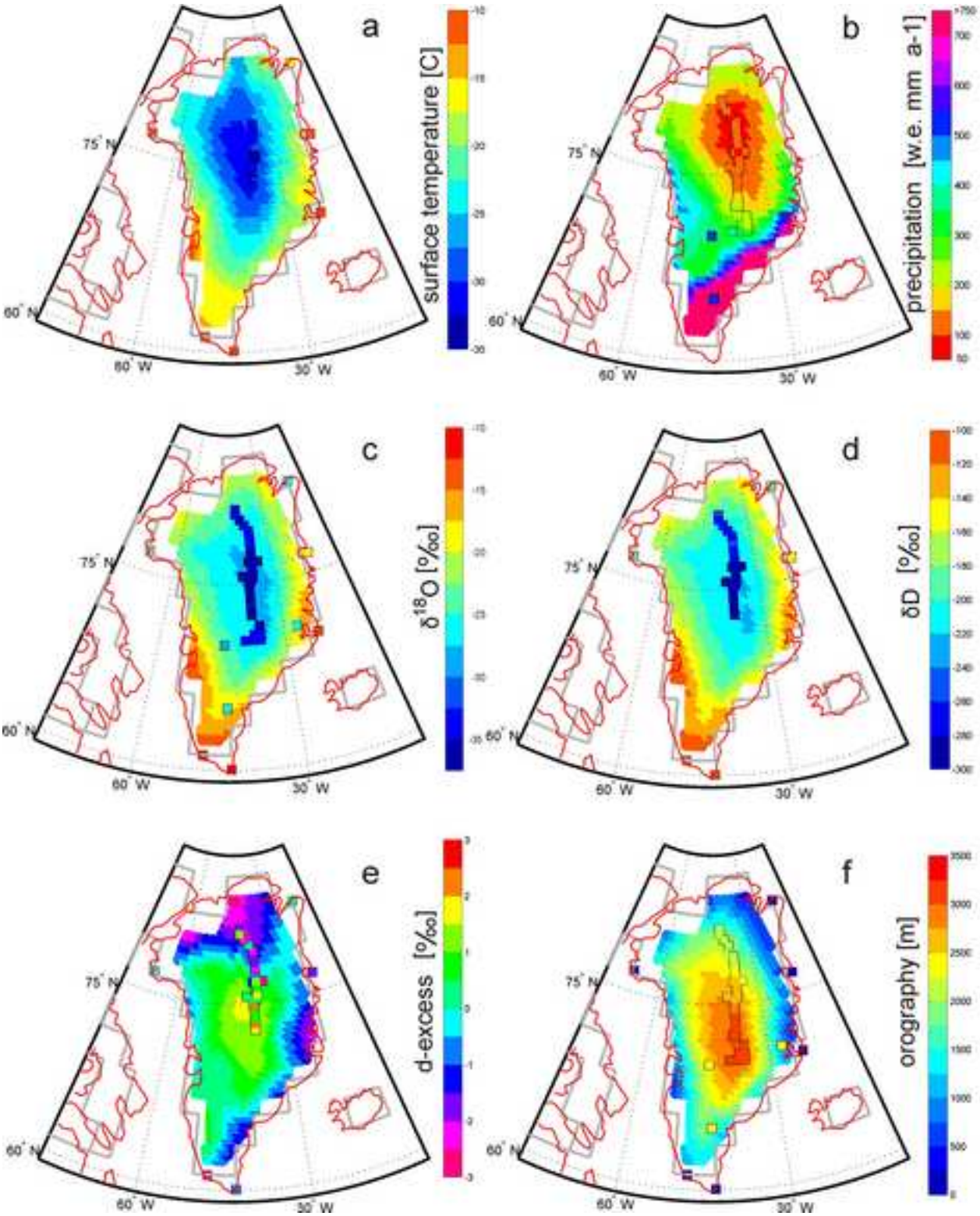

*Figure
Click here to download high resolution image

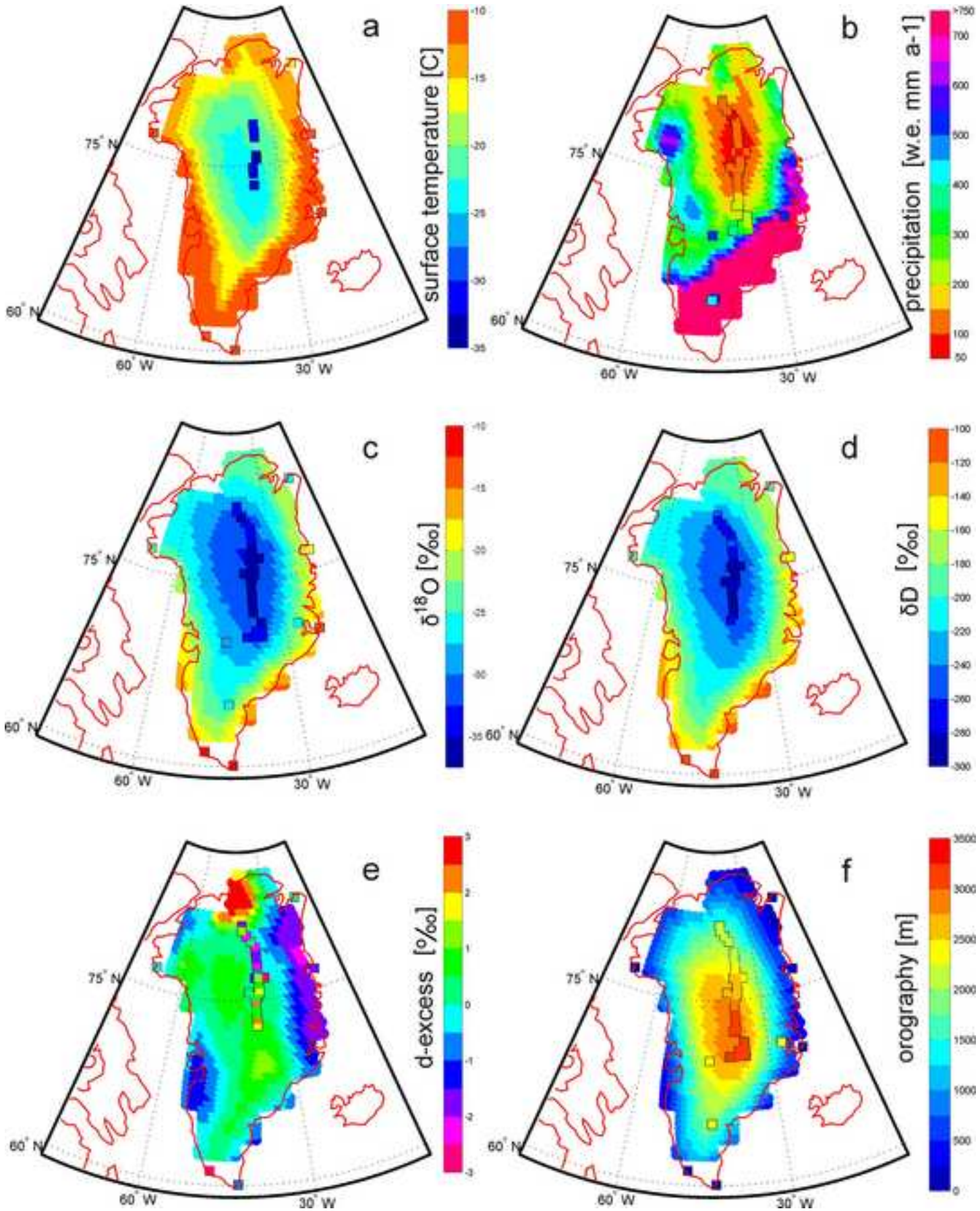

*Figure

Click here to download high resolution image

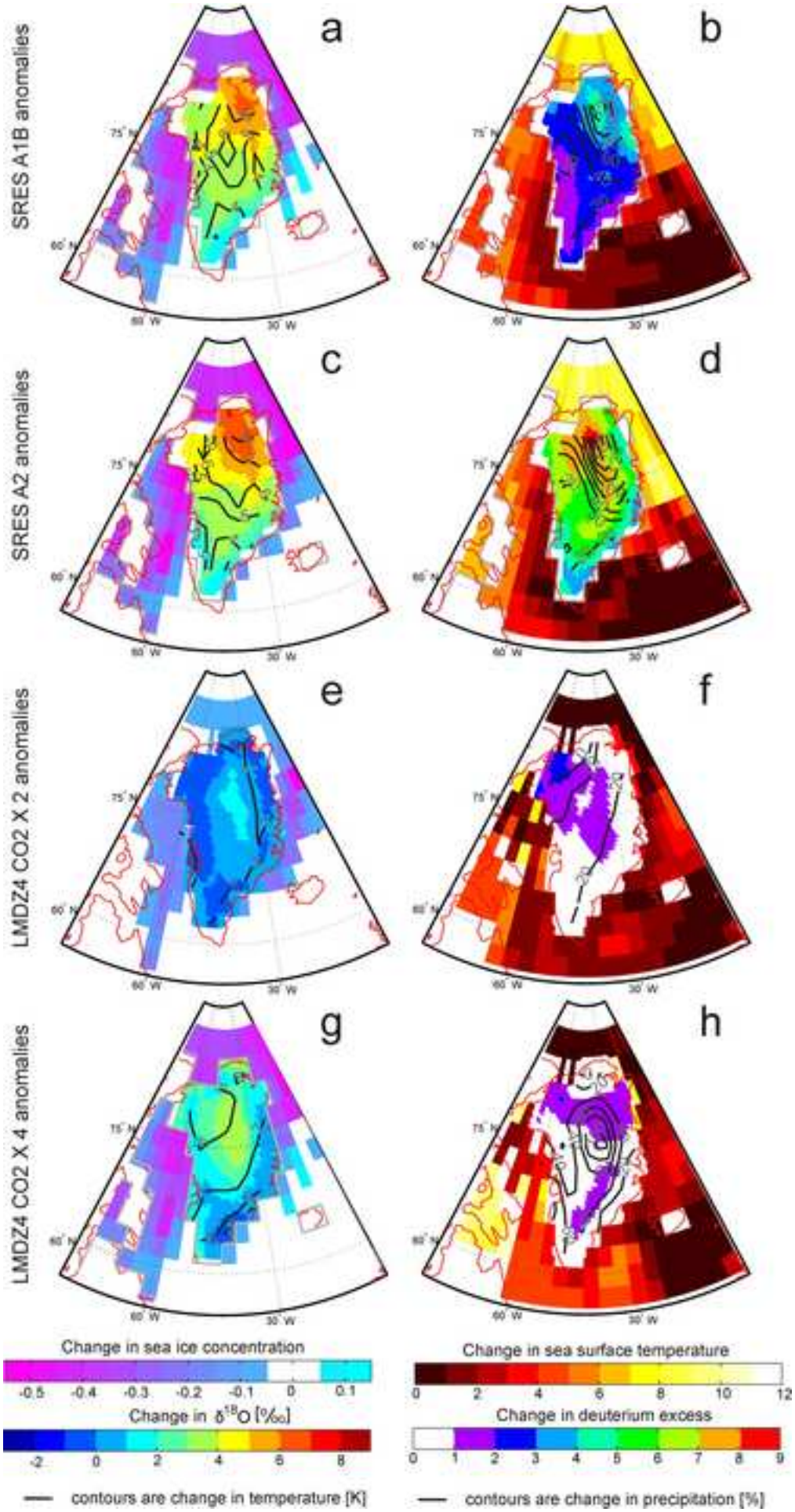

*Figure
Click here to download high resolution image

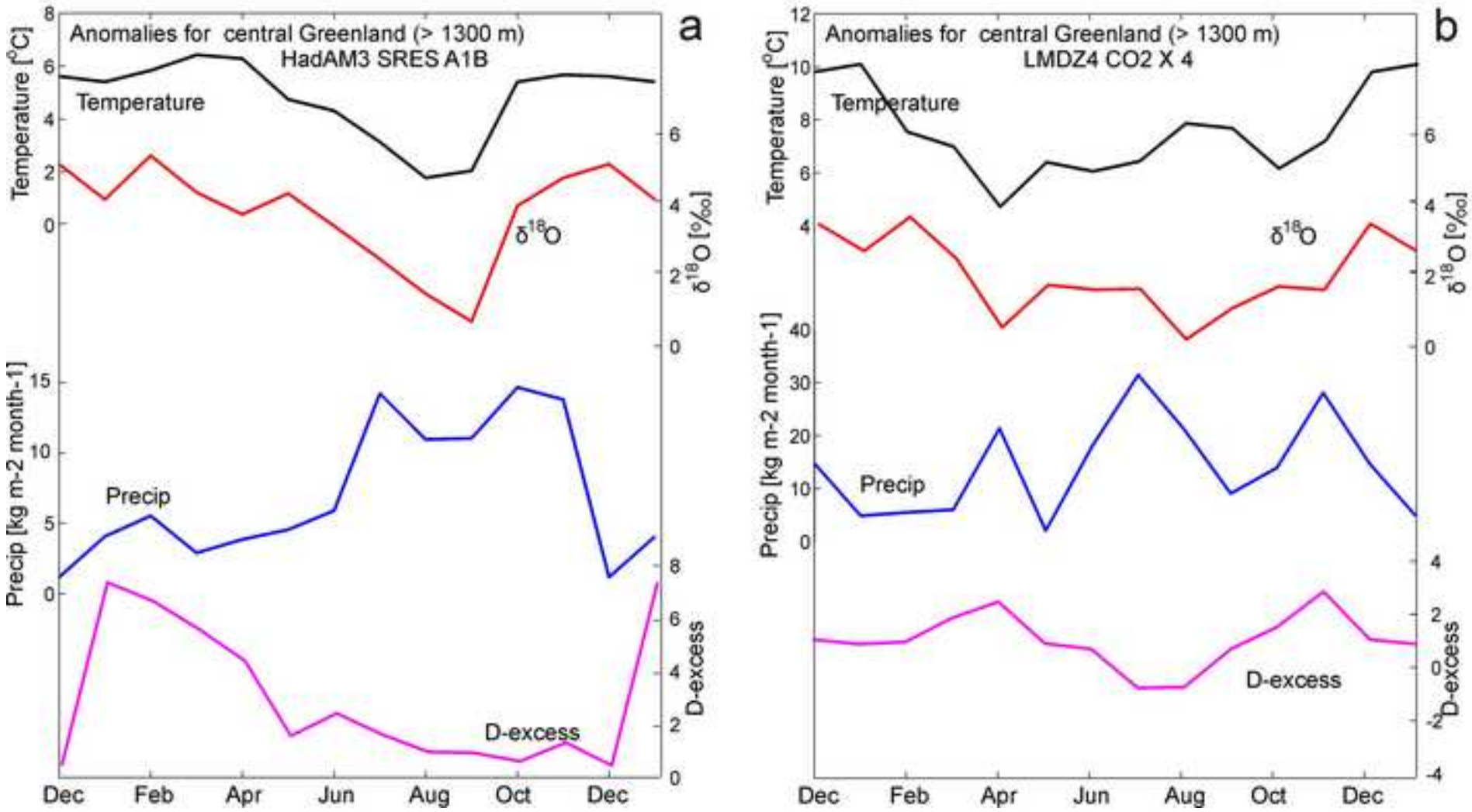

*Figure
Click here to download high resolution image

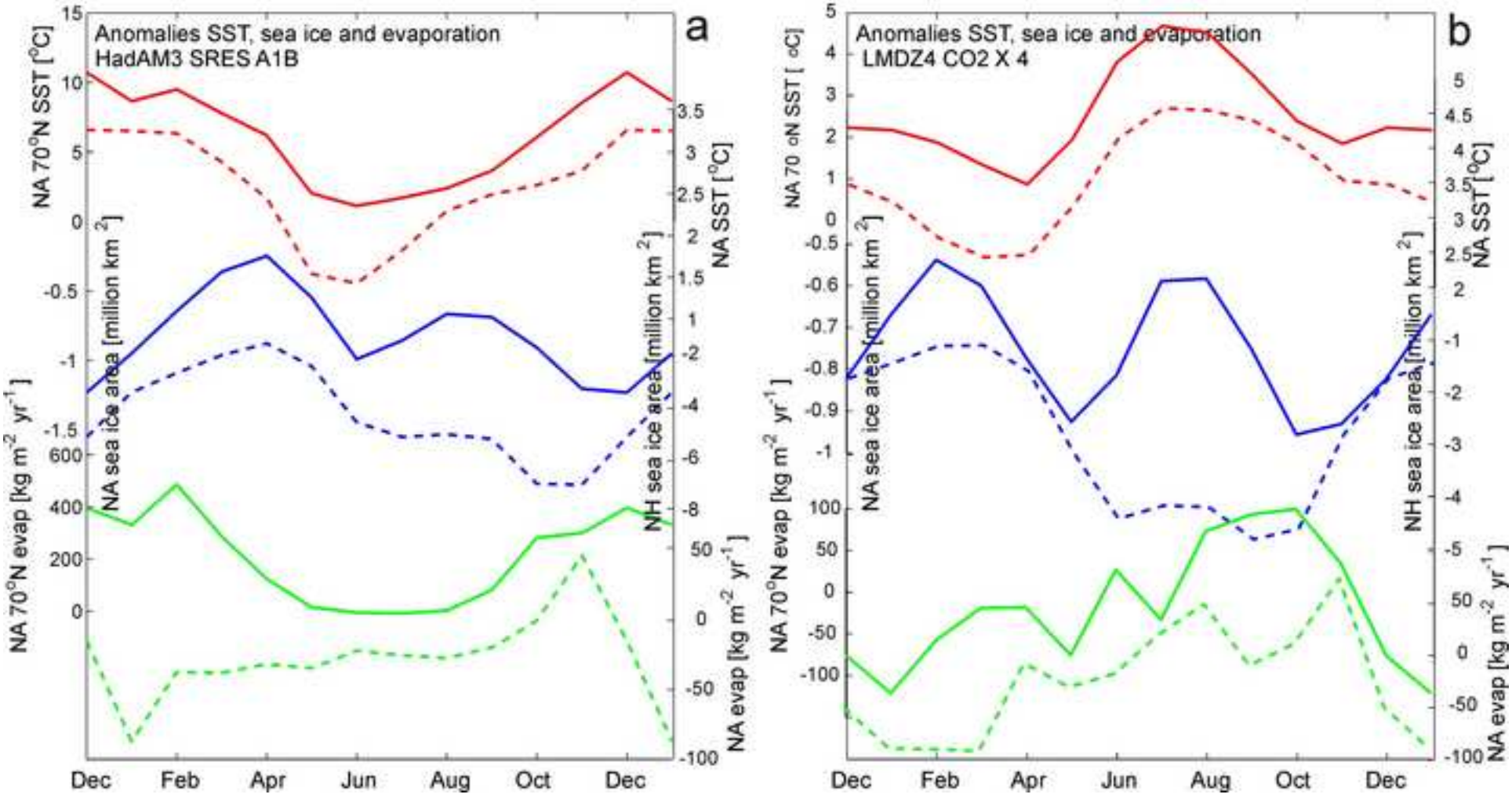

*Figure
Click here to download high resolution image

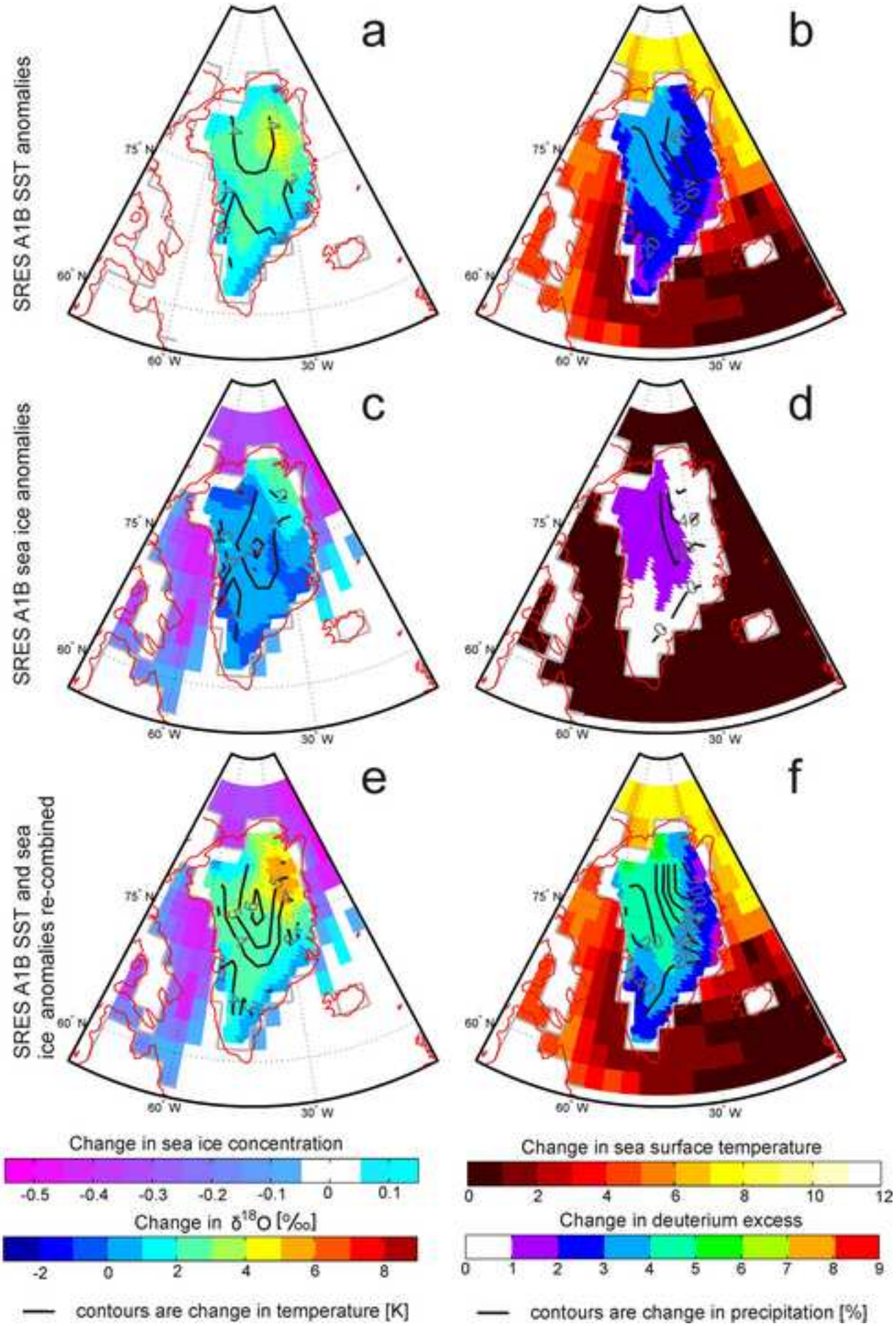

*Figure
Click here to download high resolution image

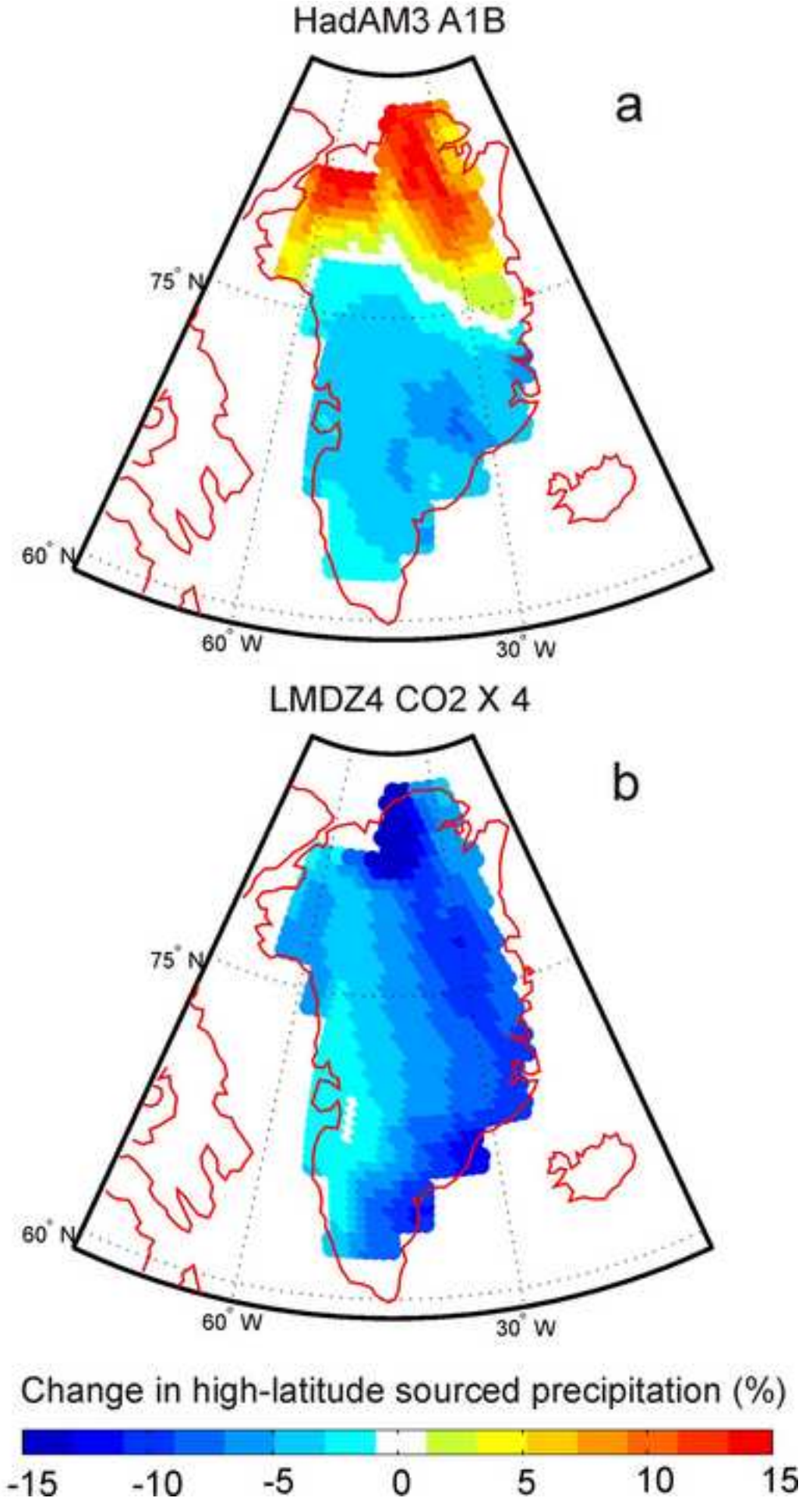

*Figure
Click here to download high resolution image

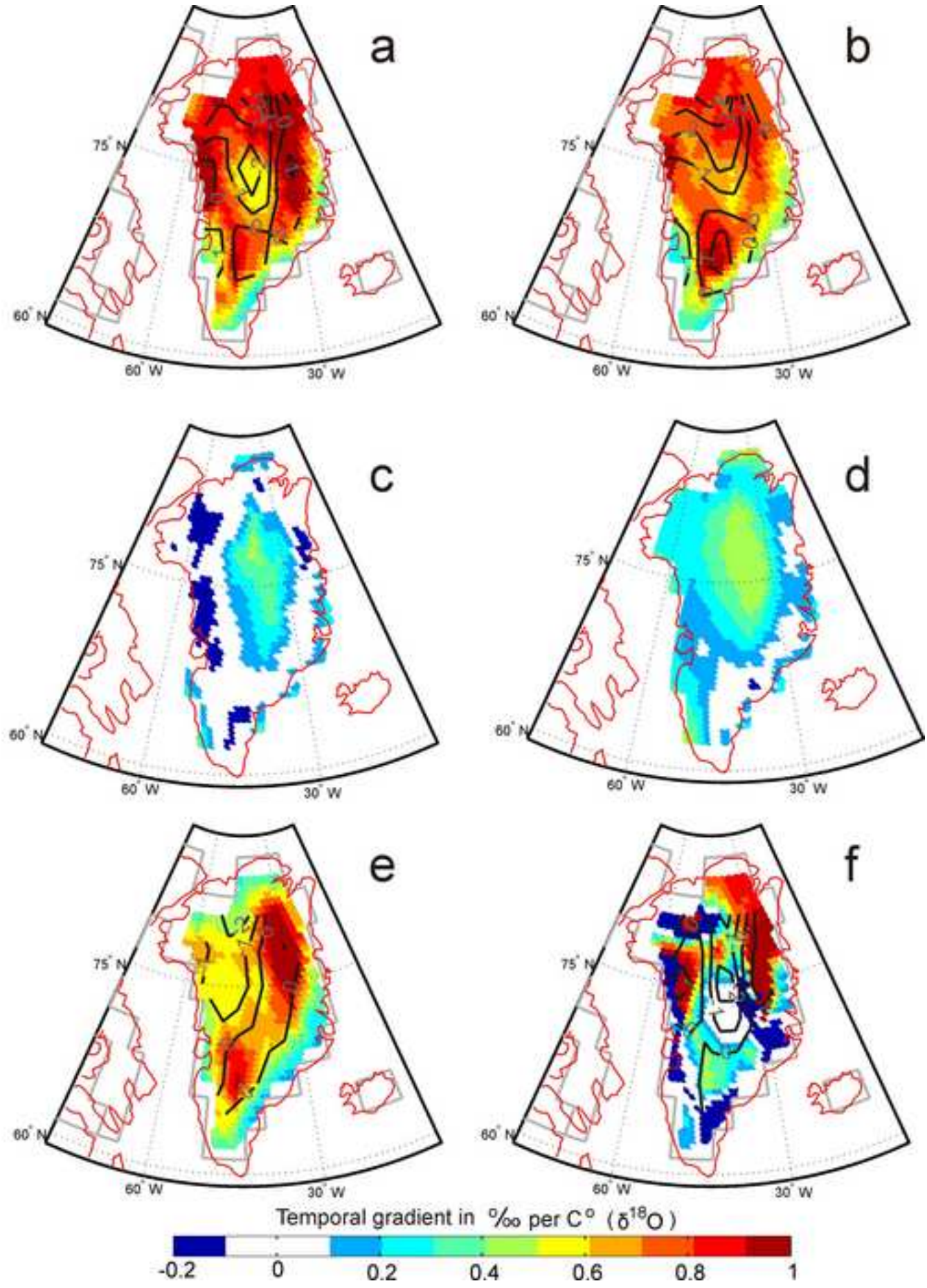

*Figure
Click here to download high resolution image

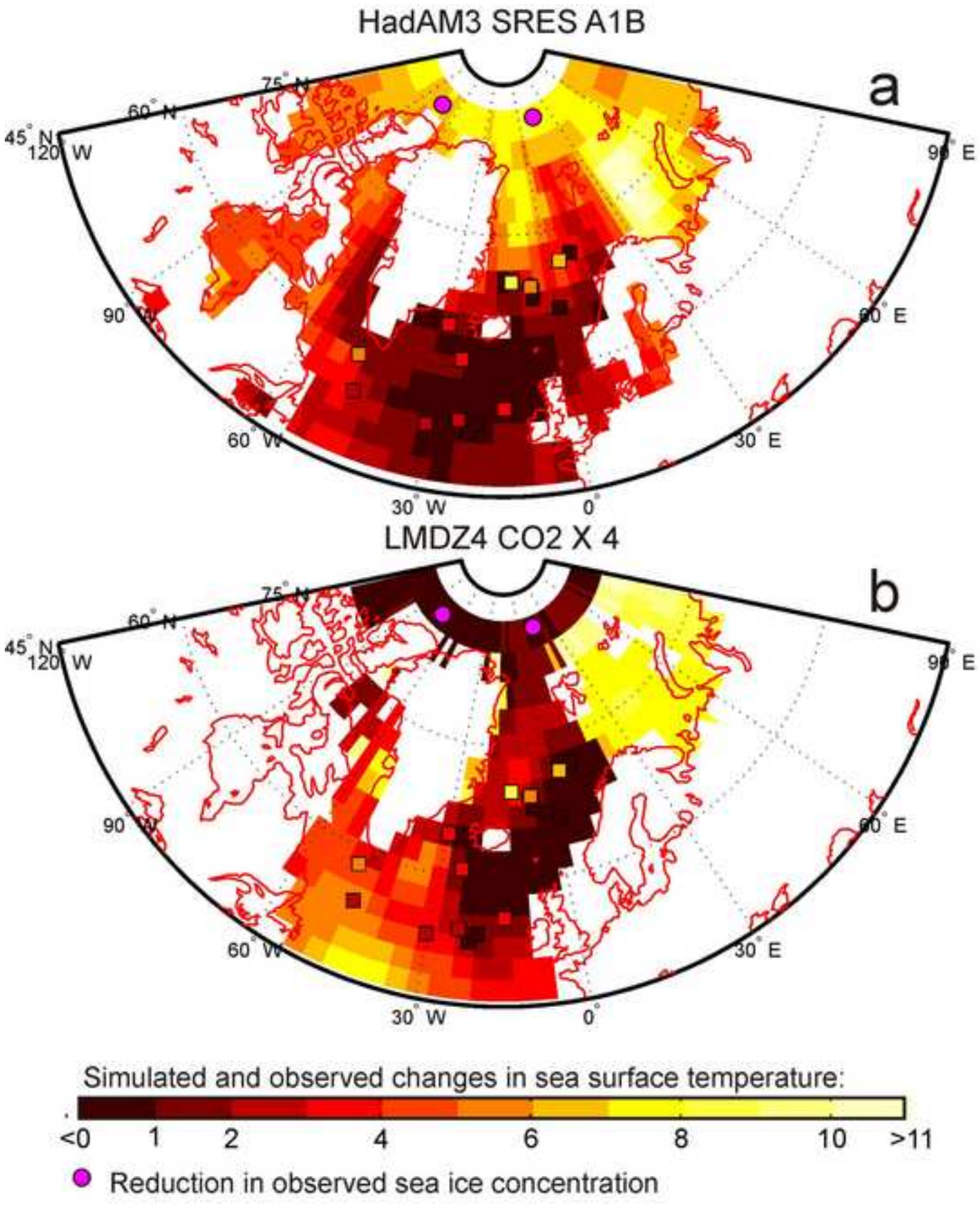

*Figure
Click here to download high resolution image

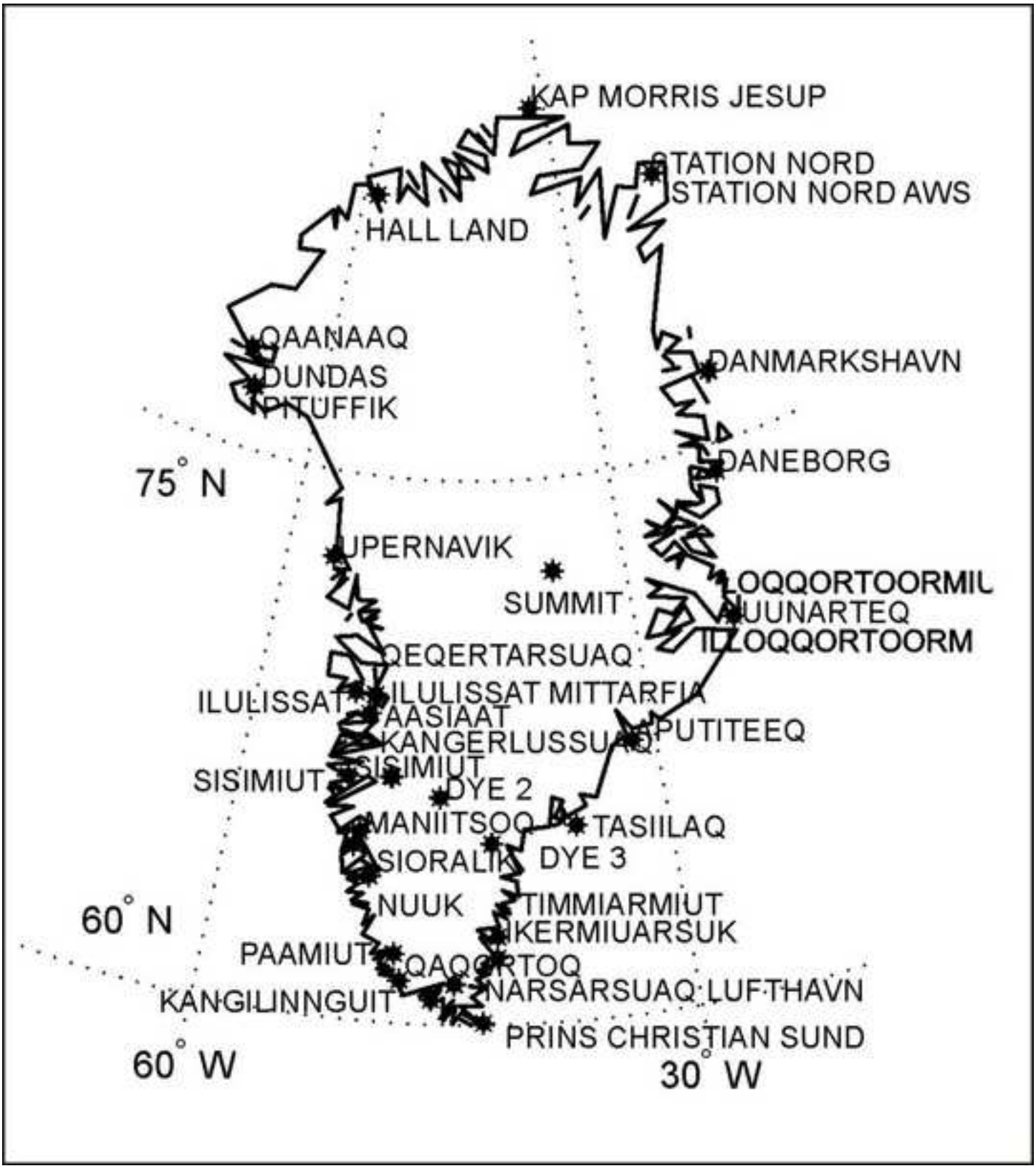

*Figure

Click here to download high resolution image

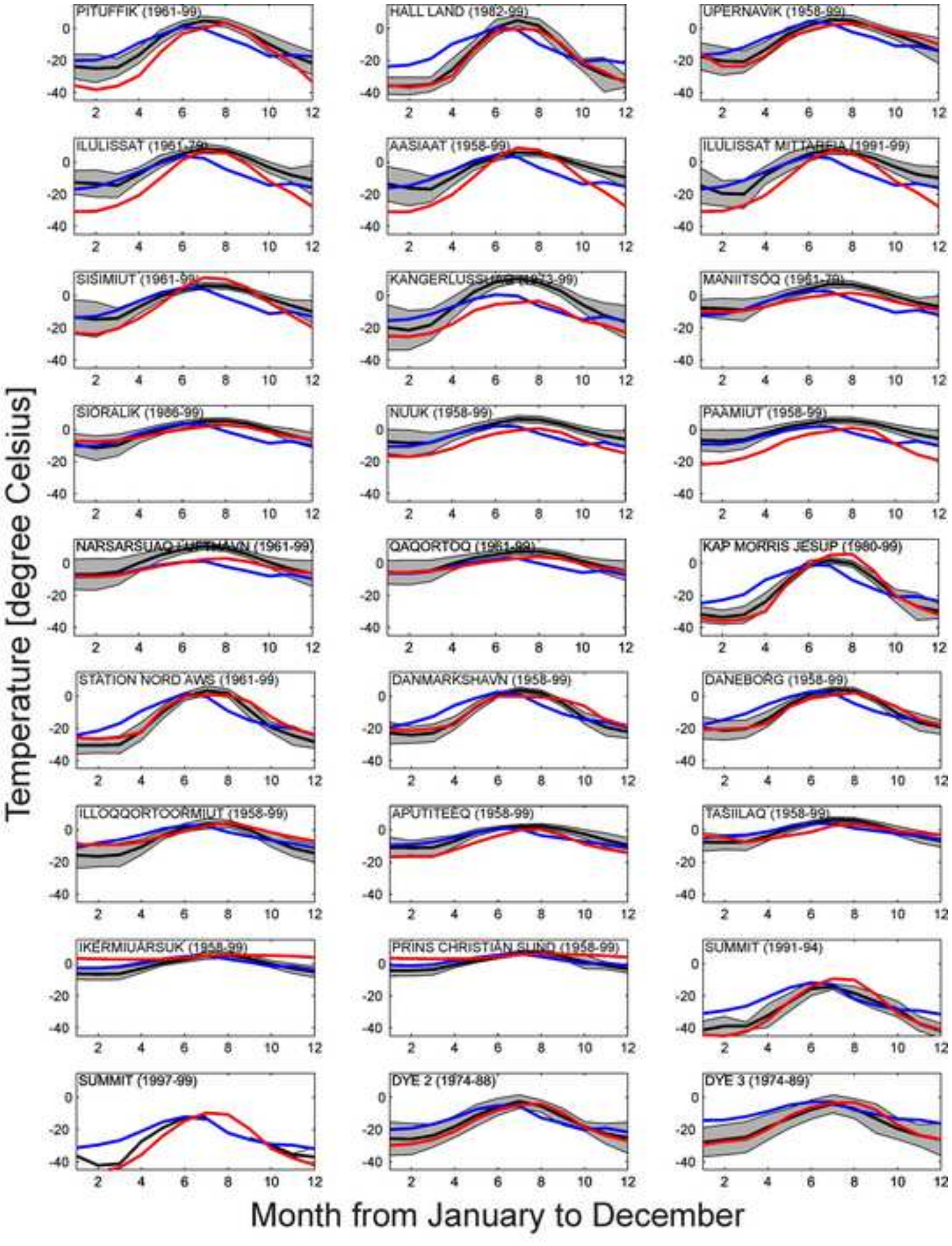

*Figure

Click here to download high resolution image

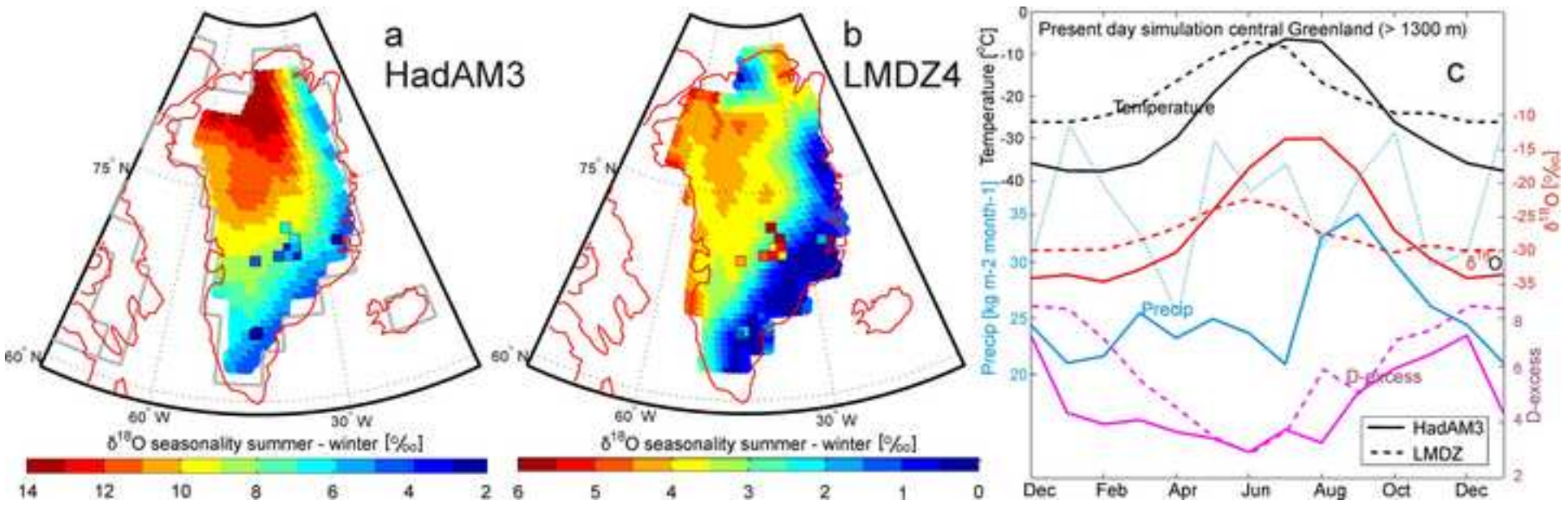

*Figure
Click here to download high resolution image

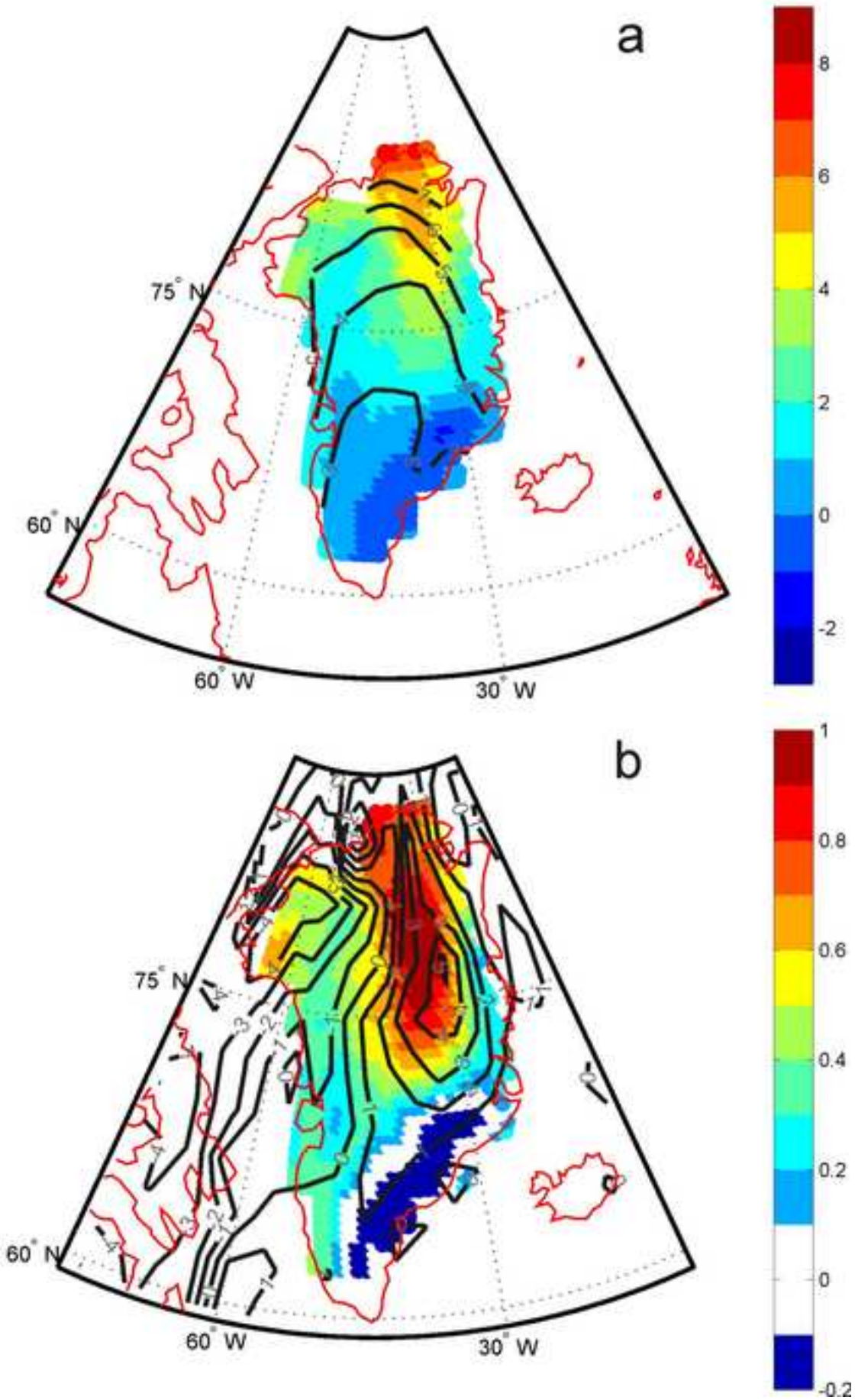

*Figure

Click here to download high resolution image